To the Graduate Council:

I am submitting herewith a thesis written by Robert C. Wolfe entitled "An Investigation of the Effects of Upstream Mass Injection on Cavity Oscillations." I have examined the final copy of this thesis for form and content and recommend that it be accepted in partial fulfillment of the requirements for the degree of Master of Science, with a major in Mechanical Engineering.

Ahmad D. Vakili

Ahmad D. Vakili, Major Professor

We have read this thesis and recommend its acceptance:

Frank G. Collins

[illegible]

Accepted for the Council:

C. W. Minkel

Associate Vice Chancellor and Dean of The Graduate School

STATEMENT OF PERMISSION TO USE

In presenting this thesis in partial fulfillment of the requirements for a Master's degree at The University of Tennessee, Knoxville, I agree that the Library shall make it available to borrowers under rules of the Library. Brief quotations from this thesis are allowable without special permission, provided that accurate acknowledgment of the source is made.

Permission for extensive quotation from or reproduction of this thesis may be granted by my major professor, or in his absence, by the head of Interlibrary Services when, in the opinion of either, the proposed use of the material is for scholarly purposes. Any copying or use of the material in this thesis for financial gain shall not be allowed without my written permission.

Signature ____________________

Date January 3, 1995

AN INVESTIGATION OF THE EFFECTS OF UPSTREAM MASS INJECTION ON CAVITY OSCILLATIONS

A Thesis
Presented for the
Master of Science
Degree
The University of Tennessee, Knoxville

Robert C. Wolfe

May 1995

ACKNOWLEDGMENTS

Many people have helped me in the pursuit of my degree. I would like to first thank my advisor, Dr. Ahmad Vakili, for his help and patience. I would also like to thank my family, and in particular, my parents, Stephen and Phyllis Wolfe, for their much appreciated support. I certainly could not have succeeded without the staff of the Gas Dynamics Lab, Dick Ray, Ricky Meeker, Harold Sartin, and Jim Goodman. I also wish to thank Paul Nagle for his help. Finally, I wish to thank the remaining members of my committee, Dr. Frank G. Collins and Dr. Ching-Fang Lo.

ABSTRACT

The experimental effort attempted to determine the effect mass injection had on the amplitude of cavity pressure oscillations using varying amounts of injection and different injection patterns. The boundary layer was also traversed by a cone probe at several locations to determine the effect of mass injection on the boundary layer profiles. Finally, a computational simulation of the experimental setup was conducted.

Results have shown that a more uniform injection with a higher blowing parameter produced the greatest reduction in the cavity pressure oscillations. The probe traverse measurements were successful except directly behind the injection surface. The computational simulation has shown shear layer movement but a spectrum analysis of the static pressures in the cavity indicated only random fluctuations.

TABLE OF CONTENTS

LIST OF FIGURES

Figure | Page

NOMENCLATURE

A^+	Van Driest constant
A_{pinj}	Area circumscribing the injection holes
B	Blowing parameter
B_c	Cavity blowing parameter
B_d	Injection blowing parameter
C_f	Coefficient of skin friction
C_p	Coefficient of pressure
D	Depth of cavity
d	distance
d^+	adjusted distance
E	Energy per unit volume
$\hat{F}$	vector
f	frequency
$\hat{G}$	vector
i	indice
J	Jacobian
j	indice
K	vortex to freestream velocity ratio, coefficient of thermal conductivity
k	ratio of specific heats
L	length of cavity
L/D	length to depth ratio
L/W	length to width ratio

l	mixing length
l_o	von Kármán constant
m	mode number
Pr	Prandtl number
Pr_T	turbulent Prandtl number
P_{inj}	injection pressure
P_s	static pressure
$\hat{Q}$	vector
$\hat{q}$	heat flux vector
q	heat flux
Re	Reynolds number
T	temperature
t	time
U	Velocity, Contravariant Velocity
u	velocity
W	width of cavity
X	coordinate
x	coordinate
Y	probe height
β_r	dimensionless number
γ	acoustic wave emission delay
δ_{ij}	Kroneker delta
θ	momentum thickness
λ	second coefficient of viscosity
μ	first coefficient of viscosity
ξ	computational coordinate

ρ	density
$\hat{\tau}$	transformed viscous stress tensor
τ	viscous stress tensor
ω	vorticity

Subscripts

inj	injection
cav	cavity
∞	freestream
o	initial
w	wall
T	turbulent

CHAPTER 1

INTRODUCTION

Cavity Oscillations

Cavity oscillations are rapid, organized fluctuations in the pressure, density, and velocity of the fluid inside a cavity which has been exposed to flow over the open side of the cavity.

Cavity oscillations have been observed to occur in wheel wells[1,2], ring cavities on projectiles[3,4], slotted wind tunnel walls[5,6], aerodynamic windows[7,8], bay vents on the Space Shuttle[9], and aircraft bomb bays[10]. The oscillations can cause structural deflection[11], structural fatigue[11], strong acoustic radiation[12], increased drag[13], and poor optical characteristics for aerodynamic windows[14].

The flow over a rectangular cavity is shown in figure 1. The external flow produces a boundary layer upstream of the cavity. The boundary layer separates at the leading edge of the cavity, forming a free shear layer. The free shear layer traverses the cavity, and reattaches at the trailing edge. The geometric variables used in this thesis will be defined as shown in figure 1-1.

The mechanism producing cavity oscillations consists of the creation of a free shear layer perturbation,

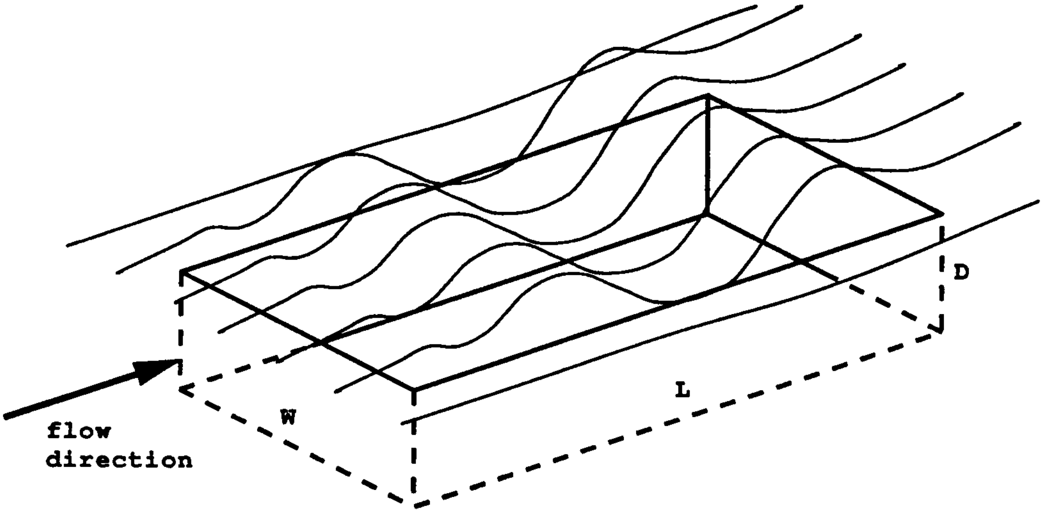

Figure 1-1 A cavity flow

amplification and downstream convection of the perturbation, interaction of the perturbation with the trailing edge structure, and production of an upstream travelling influence[15]. The perturbation is a product of the inherently unstable nature of free shear layers. The perturbation may manifest itself as an oscillation of the free shear layer, a vortex, or other vorticity fluctuation[16,17]. The perturbations are convected downstream and amplified as they convect. The amplification is selective and non-linear[43]. Upon reaching the trailing edge, the amplified perturbation interacts with the trailing edge structure and produces an upstream traveling influence. The upstream traveling influences are generally pressure disturbances, and may travel through the cavity, the free shear layer, and the freestream (when subsonic). Remembering the instability of free shear layers, the upstream traveling influence may create further free shear layer perturbations, usually at or near the separations point[18]. When the upstream traveling influence and the downstream convecting perturbations are in proper phase, resonance may occur. The resonance may produce very high amplitude unsteadiness inside the cavity.

Cavity flows are classified several ways. The simplest is to divide the cavities depending on the longest dimension of the cavity. Shallow cavities have their longest dimension in the streamwise direction. Deep cavities have their longest dimension perpendicular to the streamwise direction. The two situations are shown in figure 1-2.

Chen[19] has classified cavity flows depending on where the shear layer reattaches. In closed cavities the shear layer reattaches to the cavity floor and subsequently separates before finally reattaching to the trailing edge. In open cavities the shear layer is free across the cavity and reattaches at the trailing edge. Chen found that the cavity flow was closed for length-to-depth (L/D) ratios over approximately thirteen, that the cavity flow was open for L/D ratios below around 10, and could be either open or closed for L/D ratios in between. The drag of closed cavities is substantially higher than that of open cavities[30].

Naudascher's[20] terminology has been used to classify cavity flows in a review paper by Rockwell and Naudascher[21]. The classifications are fluid-dynamic, fluid-resonant, fluid-elastic. The classifications as well as several examples of situations where they might occur are shown in figure 1-3.

Fluid-dynamic cavity flows occur when the acoustic wavelength is large compared to the cavity length. Both the selective amplification of perturbations as well as the creation of pressure disturbances near the trailing edge are necessary.

Fluid-resonant cavity flows are characterized by strong acoustic resonances inside the cavity. Naturally, the

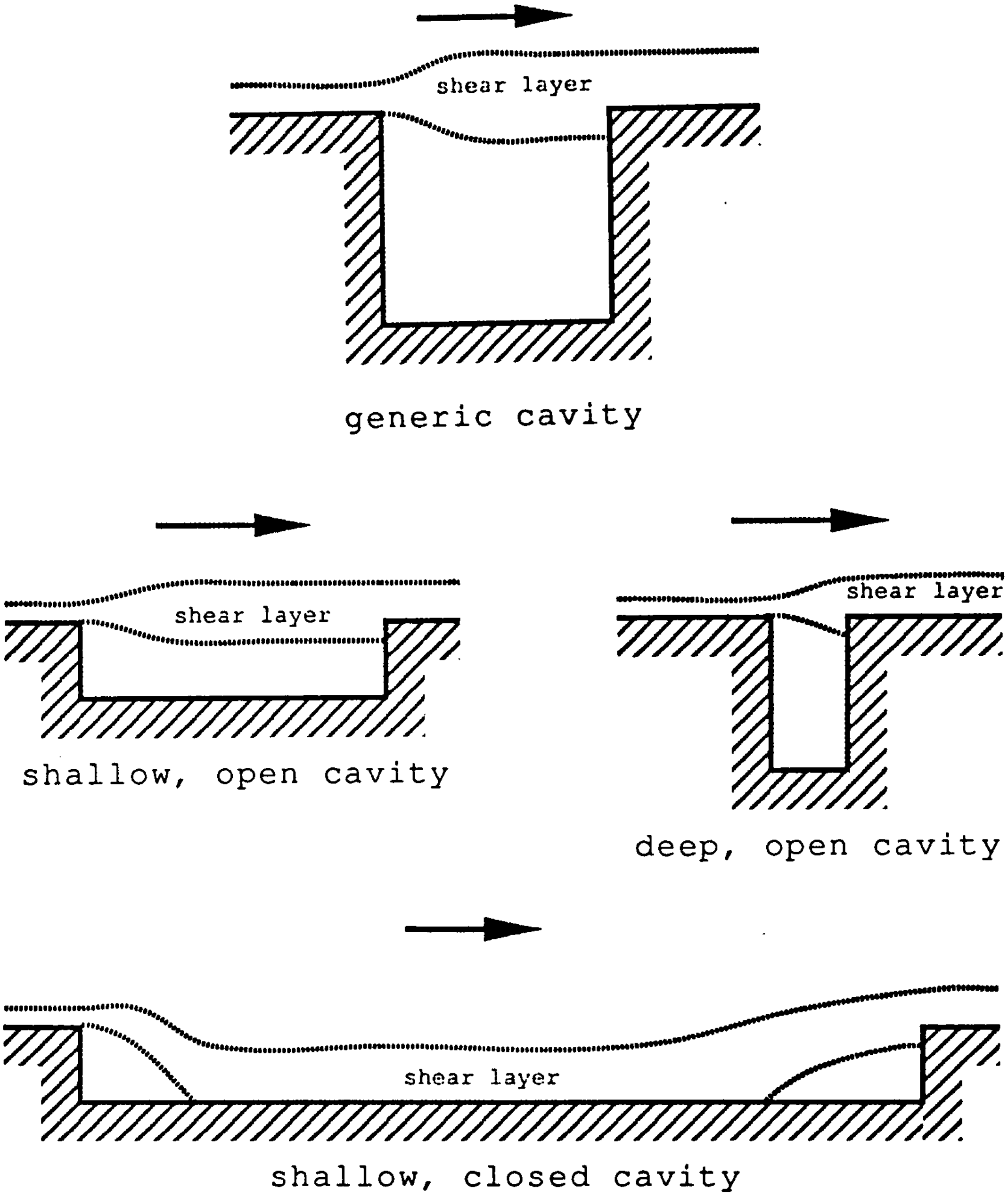

Figure 1-2 Cavity flow classifications

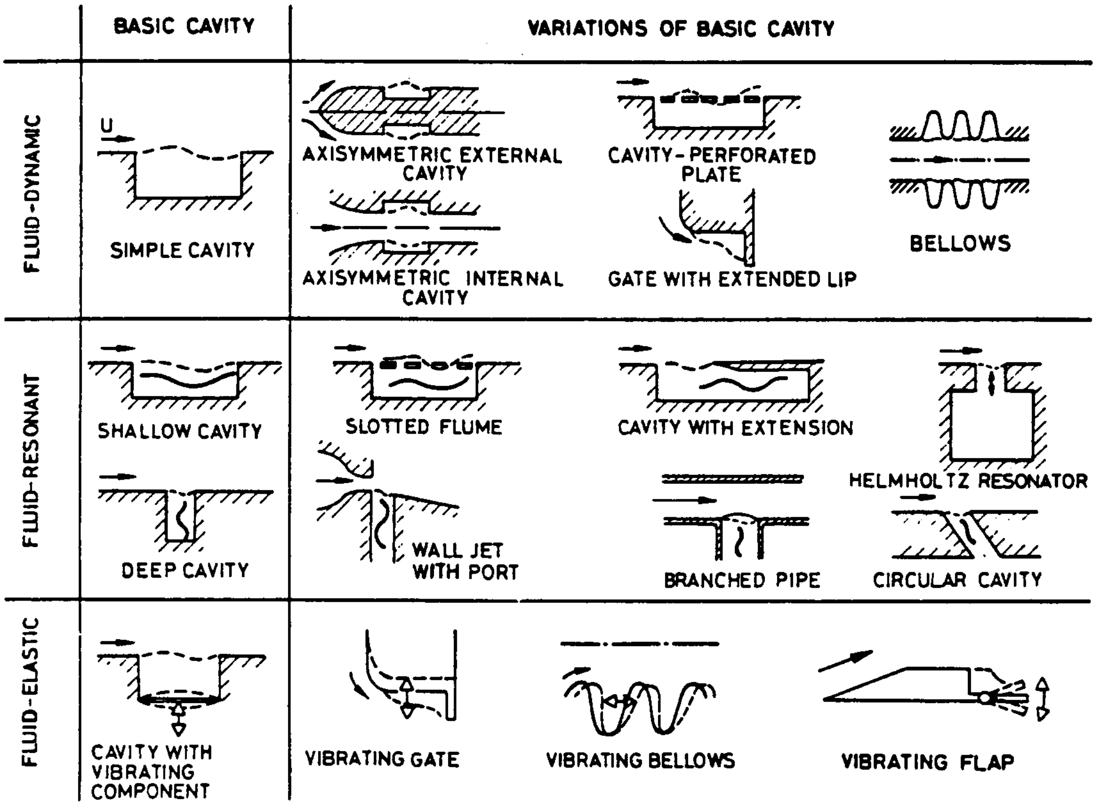

Figure 1-3 Matrix classification of cavity oscillations from Rockwell and Naudascher[21]

acoustic wavelengths are equal to or less than the relevant cavity dimension. The acoustic resonances provide the upstream traveling influence.

Fluid-elastic cavity flows are characterized by elastic deformation of the cavity structure. The vibration of the structure produces pressure and acoustic resonant effects. The structural properties of the cavity play an important role in the behavior of these cavity oscillations.

Important parameters characterizing cavity flows are the upstream boundary layer parameters, free shear layer parameters, cavity geometry parameters, and freestream parameters. Figure 1-4 shows some of these parameters.

Suppression Efforts

Cavity oscillations are occasionally considered desirable, but researchers have usually sought to suppress them. Many different ways have been tried to reduce or eliminate the oscillations. The different attempts at suppression may be categorized by the part of the cavity flow they seek to directly alter. The categories are direct and indirect free shear layer alteration, separation and reattachment alteration, and upstream boundary layer alteration.

Direct and indirect free shear layer alteration includes passive venting of the cavity floor[22], mass injection through the cavity floor[23], and the presence of solid

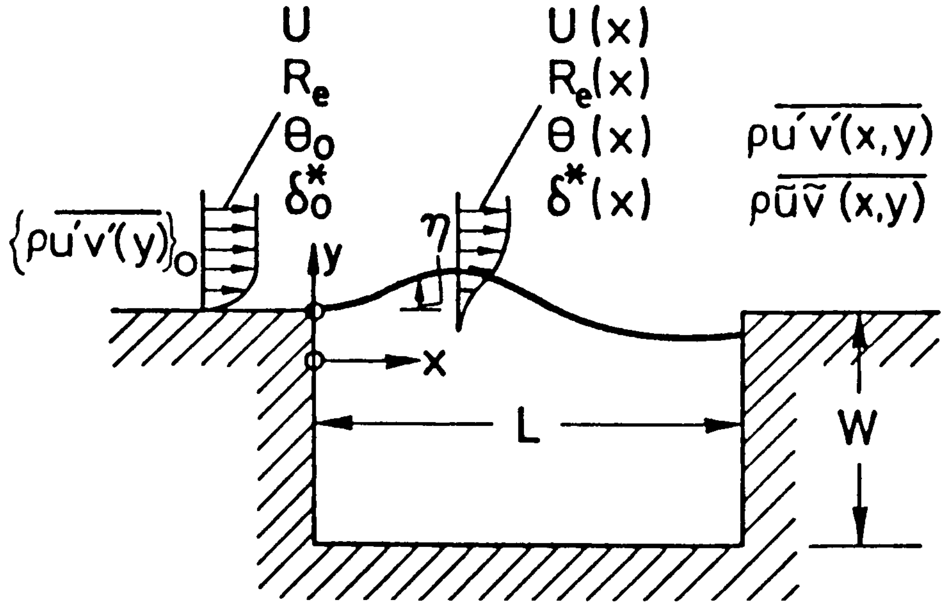

Figure 1-4 Important parameters in cavity flows from Rockwell and Naudascher[21]

objects inside the cavity, but touching the shear layer[24].

Separation and reattachment alteration includes leading and trailing edge structural modifications such as ramps[24]. This technique has been studied extensively.

Upstream boundary layer alteration includes cowls[17], vortex generators[25], spoilers[25], pin arrays[26], and upstream mass injection[27,28].

Combinations of the above approaches are also possible. The technique showing the greatest promise for the attenuation of cavity oscillations over a broad range of free stream mach numbers is upstream mass injection.

Mass Injection

Mass injection into a boundary layer may be achieved in several ways. The mass may be injected parallel to the flow, transverse to the flow, or at any angle in between. The injection may take place through discrete holes, slots, screens, sintered surfaces, or other porous surfaces. The injection may be uniform over an area or non-uniform. Finally, the injection may be steady or unsteady. Only uniform, steady, transverse injection will be discussed further.

The effects of transverse injection depend mostly on the relative momentum or the relative mass flux of the injected flow to the free stream flow. The blowing parameter is defined by $B = (\rho_{inj}u_{inj}/\rho_{\infty}u_{\infty})$. Low rates of injection produce only modest effects on the boundary layer profile or the freestream flow[29]. Large rates of injection produce significant changes in the boundary layer velocity profile and the freestream[36]. Very large rates of injection may produce separation of the injected mass and the boundary layer[29]. The changes produced by mass injection also include the thickening of the boundary layer, increases in the momentum thickness and displacement thickness, and the formation of shocks when the free stream is supersonic[29,36].

The purpose of boundary layer mass injection upstream from a cavity is to alter the characteristics of the boundary layer. Because the free shear layer over a cavity is formed from the separated upstream boundary layer, changes in the boundary layer could be expected to result in changes in the free shear layer. When the changes in the free shear layer interfere with or suppress the mechanism causing cavity oscillations, a reduction in the cavity oscillation amplitude is possible.

Computational Cavity Flow Simulation

The complexity of cavity flows and the lack of a comprehensive analytic model leads to the consideration of numerical or computational approaches. The fundamentals of computational fluid dynamics will not be discussed here. However, cavity flows have been simulated by computer with varying degrees of success and the general approach used in this thesis will be described.

Computational simulations may be based on any of several sets of fluid dynamics equations. For example, the potential, Euler, and different versions of the Navier-Stokes equations are all in present use. The Navier-Stokes equations are the most general and the most useful for complex flows. They can be solved in either two or three dimensions. The Navier-Stokes equations apply equally well for laminar and turbulent flows. Unfortunately, turbulence operates at scales below practical computational resolution. As a result, the Reynolds averaged Navier-Stokes equations, with the addition of external models of turbulence to induce closure of the equation system, are required. These turbulence models are semi-empirical, including algebraic models and the popular k-ε model.

Thesis scope

The focus of this thesis will be an examination of the effect of upstream mass injection on the flow over a shallow, open cavity at a nominal Mach number of 1.75 and the effectiveness of upstream mass injection in reducing cavity oscillations. The cavity L/D ratio is 4.33 and the cavity length-to-width (L/W) ratio is also 4.33. A two dimensional computational simulation of the cavity will also be conducted.

CHAPTER 2

LITERATURE REVIEW

Cavity Oscillations

The phenomenon of cavity oscillations was specifically studied by Krishnamurty in 1955. Krishnamurty[12] investigated small, two dimensional cavities (0.1" to 0.3" in depth by 0" to 2" in length) at Mach numbers from 0.25 to 1.5. He observed the strong acoustic radiation emitted by the cavity, and that the radiation was more intense for a laminar upstream boundary layer than for a turbulent upstream boundary layer. Krishnamurty also found that a minimum length existed for oscillations to occur and that the length was inversely proportional to the Mach number.

Roshko[13] studied the pressure and velocity fields produced by low speed flows (75 ft/s to 210 ft/s) and cavities measuring 0" to 10" in depth by 4" in length. He noted that the cavity flow was open for L/D ratios less than or equal to ten. He also determined that the increased drag of cavities is almost entirely due to the pressures induced on the cavity walls by the cavity flow. Roshko suggested that shear layer impact on the cavity trailing edge might be important in the sound production by cavities.

Plumblee, Gibson, and Lassiter[31] examined cavities with L/D ratios from 0.5 to 1.5 at Mach numbers from 0.2 to

5.0. Plumblee et al. concluded that deep cavities resonate primarily in the depth modes and shallow cavities primarily in the lengthwise modes. They suggested that the resonances were driven by the broadband turbulent fluctuations and modeled the cavity as an acoustic resonator. Krishnamurty's observations of acoustic radiation in cavity flows with upstream boundary layers clearly contradicts this theory.

Rossiter[17] investigated shallow cavities (0.8" to 8" in depth by 8" in length) at low and transonic Mach numbers from 0.4 to 1.2. Rossiter's high speed shadowgraph motion pictures showed the periodic emission of vortices and the downstream convection and growth of the vortices. Rossiter suggested a simple model consisting of periodic vortex emission, convection downstream, and impingement on the trailing edge. Some fraction of a period later, an acoustic wave is emitted from the trailing edge, travels upstream, and perturbs the shear layer at the leading edge. The perturbation is a vortex, thus completing the cycle. This model predicts all possible frequencies of resonance but not which frequency will occur. The empirical formula obtained by Rossiter is:

$$f=\left(\frac{U_\infty}{L}\right)\cdot\left(\frac{m-\gamma}{M_\infty+\frac{1}{K}}\right)$$

where f = frequency

L = cavity length

U_∞ = freestream velocity

M_∞ = freestream Mach number

m = mode number (1,2,3,...)

K = vortex to freestream velocity ratio

γ = acoustic wave emission delay

The acoustic wave emission delay is an empirical constant intended to represent the lag between vortex impingement on the trailing edge and the emission of an acoustic wave. Rossiter also suggested the importance of the ratio of the boundary layer thickness to the cavity depth and noted the similarity of some aspects of cavity oscillations to the jet edgetone phenomena, in particular the presence of stages or modes of oscillation.

Heller, Holmes, and Covert[32] studied shallow cavities with L/D ratios from 4 to 7 at Mach numbers from 0.8 to 3.0. They improved on Rossiter's formula with respect to the speed of sound inside the cavity. Rossiter assumed the cavity sonic speed equalled the free stream sonic speed. Heller et al. suggested using the stagnation sonic speed. Their modification is:

$$f=\left(\frac{U_\infty}{L}\right)\cdot\left(\frac{m-\gamma}{\frac{M_\infty}{\sqrt{1+\frac{k-1}{2}M_\infty^2}}+\frac{1}{K}}\right)$$

where k = ratio of specific heats

Heller et al. noted that shallow cavities make poor resonators and must be driven strongly. They offered the trailing edge of the cavity as a reasonable location for the driver. Finally, they emphasized that the boundary layer parameters must be included in any complete theory of cavity oscillation amplitudes.

Bilanin and Covert[33] developed a model of cavity oscillation that consisted of a vortex sheet and a single, periodic acoustic monopole located at the trailing edge. The analysis of the vortex sheet stability combined with the interior acoustic field created by the monopole yielded a result similar in form to Rossiter's formula, but lacking the empirical constants.

Heller and Bliss[25] proposed a physical mechanism for cavity oscillation involving the interaction of the free shear layer and traveling pressure waves inside the cavity. The pressure waves force the shear layer to oscillate, alternately adding and ejecting mass from the cavity. Heller and Bliss termed this the "psuedopiston" effect. They also conducted an experimental effort for cavities with L/D ratios between 2.3 and 5.5 and at Mach numbers from 0.8 and 2.0.

Sarohia[34] examined ring cavities with dimensions of 0.05" to 0.875" in depth and 0" to 2" in length at speeds between 0 ft/s and 80 ft/s. Sarohia found a non-dimensional minimum length for oscillations to occur in laminar flows when the depth to boundary layer thickness ratio is greater than two. He observed the large oscillation of the free shear layer transverse to the flow direction at the trailing edge and found that the perturbations propagated through the shear layer at a constant phase speed.

Tam and Block[16] investigated cavities with L/D ratios of 0.783 and 2.348 at Mach numbers between 0.05 and 0.4. They suggested that normal mode resonance dominated at Mach numbers below 0.2 even for the shallow cavity. Tam and Block also developed a mathematical model for predicting possible oscillation frequencies. They criticized Rossiter's formula as not accurately describing all the experimental evidence. They also criticized the vortex sheet model of the free shear layer used by Bilanin and Covert[33] as not accounting for finite free shear layer thickness. Tam and Block's model accounted for acoustic emission at the trailing edge as well as acoustic reflections from the front, back, and bottom of the cavity. Their model also accounted for the finite thickness of the shear layer. Based on this model they suggested that the ratio of the cavity length and momentum thickness of the shear layer was important. Their model worked well for Mach numbers above 0.2 and below 0.4.

Suppression efforts

Rossiter[17] noticed that the frequency spectrums differed significantly for two cavities of the same L/D ratio when one cavity was half the size of the other. He concluded that differing boundary layer thickness relative to cavity size was responsible. Rossiter then attached three solid spoilers to the leading edge of a cavity with a L/D ratio of 1 to see if the alteration of the flow over the cavity caused by the spoilers would suppress the pressure fluctuations. He was somewhat successful in reducing the oscillation amplitude, with the largest spoiler producing the greatest decrease.

Buell[8] investigated antiresonance devices for deep cavities with circular openings at Mach numbers from 0.57 to 0.87. He tried porous spoilers of various porosities, a high aspect ratio diffuser feeding a porous spoiler, a cambered low aspect ratio diffuser feeding a porous spoiler wrapped partway around the circular opening of the cavity, and the wrap around porous spoiler without the cambered diffuser. He found almost complete suppression of the pressure fluctuations for the 35% porous spoiler. Buell also measured velocity profiles which showed that the spoiler created a low velocity, low velocity gradient fluid layer between the freestream flow and the cavity recirculation region.

Heller and Bliss[25] tried several suppression techniques; upstream vortex generators, trailing edge modification, and trailing edge cowl. For a cavity with a L/D ratio greater than four, a trailing edge ramp reduced the cavity oscillation amplitude for Mach numbers between 0.8 and

2.0. For cavities with L/D ratios less than four, upstream vortex generators were necessary to obtain the reduction. The trailing edge cowl also improved the performance of the trailing edge ramp. However, the position of the cowl depended critically on the free stream Mach number in order to assure the optimum suppression.

Franke and Carr[24] studied numerous geometrical modifications in a water tunnel. Promising configurations were further studied in air flows at a Mach number of 1.6. Modifications that looked promising in the water tunnel were: placing a baffle near the trailing edge, stores inside the cavity but touching the free shear layer, airfoil cowl at the leading edge, and ramps at the leading and trailing edge. The double ramp configuration worked reasonably well in the air flow tests. However, effective suppression required that the upstream boundary layer separate at the front of the leading edge ramp. Separation at the rear of the leading edge ramp produced increased oscillation amplitude. In addition, the broadband pressure fluctuations generally increased for successful suppression efforts.

Sarohia and Massier[23] attempted to suppress the cavity oscillations occurring in a ring cavity at Mach numbers from 0 to 0.5 by steady injection of mass into the base of the cavity. They observed a reduction in pressure and velocity fluctuations as well as radiated sound. However, they also observed that the cavity oscillations were sometimes enhanced through slight unsteadiness in the mass injection. The injected mass necessary to suppress the cavity oscillations was from B = 0.05 to B=0.15.

Smith, Gutmark, and Schadow[26] looked at the success of several techniques for the suppression of cavity oscillations. Multiple leading edge steps, ramps, V grooves perpendicular to the streamwise flow, and trailing edge pins were not successful. Leading edge pins were found to be the most effective at Mach numbers of 1.8 and 2.6. The pins were mounted upstream of the cavity leading edge, perpendicular to the surface, in a line between 30° and 45° relative to the streamwise direction, spaced uniformly across the width of the cavity leading edge width. This configuration yielded significant attenuation of approximately a factor of 5.

Sarno and Franke[35] investigated static and oscillating upstream boundary layer fences and steady and pulsating slot mass injection at the leading edge of a cavity with a L/D ratio of 2 and at Mach numbers from 0.6 to 1.5. The static fence was found to be most effective. However, it was only useful for suppressing the first resonance mode.

Vakili and Gauthier[28] studied the suppression of cavity oscillations by upstream mass injection through plates with numerous holes at a Mach number of 1.8 and cavity L/D ratio of 2.54. They obtained almost complete suppression of the cavity oscillations. Broadband fluctuations were also reduced. The peak amplitudes produced by the cavity were reduced from 1.5 psi to 0.07 psi. They determined that at the lower mass injection rates, low area density injection produced greater suppression. They attribute the reduction in cavity oscillations to changes in the shear layer parameters and a resulting alteration in its instability characteristics.

Mass Injection

Goldstein, Shavit, and Chen[36] studied the effectiveness of film cooling by transverse mass injection through a fine screen at speeds of 100 ft/s to 185 ft/s over a flat plate. The blowing parameter, B, was varied from 0.0078 to 0.0497. Velocity profiles were measured and boundary layer parameters calculated. Low rates of injection produced small changes in the velocity profile. Large blowing rates produced large changes in the profile, appearing to lift the boundary layer off the surface. The displacement thickness and momentum thickness both increase rapidly over the injection region, reach a maximum a short distance downstream, and then fall as the boundary layer relaxes.

Fernandez and Zukoski[29] studied injection through a surface composed of sintered particles into a flow with a Mach number of 2.6 over a flat plate. They divided mass injection into three categories; weak, massive, and blowoff mass injection. The integrated x-momentum equation for a two dimensional boundary layer with no streamwise pressure gradient and with mass injection was given as:

$$\frac{d\theta}{dx}=B\cdot(1+\frac{C_f}{2B})$$

where θ = momentum thickness

$B = \rho_{inj}u_{inj}/\rho_\infty u_\infty$

C_f = coefficient of skin friction

x = coordinate

Weak mass injection occurs when the skin friction term and the mass injection term are comparable in the above equation. Massive mass injection occurs when the mass injection term is large compared to the skin friction term, thus making the shear layer momentum thickness rate of growth primarily dependent on the injected mass, but the momentum of the injected mass is small compared to the freestream flow momentum. Blow-off mass injection occurs when the momentum of the injected mass is comparable to or greater than the freestream flow momentum. As the term "blowoff" suggests, flow separation can occur.

Fernandez and Zukoski injected mass with B varying from 0 to 0.045. Their velocity profiles show a regular progression from a typical flat plate boundary layer to the free mixing layer profile as B is increased. They propose that when B exceeds 0.03, the flow is at incipient separation.

Computational Cavity Flow Simulation

Hankey and Shang[37] attempted a two dimensional simulation of the flow over a cavity with a L/D ratio of 2.25 and Mach number of 1.5. They solved the two dimensional Navier-Stokes equations using a time dependent, alternating direction explicit scheme by MacCormack. Turbulent closure was achieved by the Cebecci-Smith eddy viscosity model with relaxation modification. The computational grid was cartesian and had dimensions of 78 x 52 points. Their time dependent results show a single cavity recirculation and orderly development of the shear layer across the cavity. Their predictions of mean static pressures are reasonable compared to the experimental data of Heller and Bliss[45]. A spectral analysis of the results show reasonable agreement for the first and second cavity oscillation modes with respect to frequency and amplitude, also compared to data from Heller and Bliss[45]. However, higher frequencies were not accurate.

Baysal and Stallings[38] also attempted a two dimensional simulation of a cavity flow. They simulated cavities with L/D ratios of 6,12,16 and a Mach number of 1.5. They solved the integral form of the two dimensional Navier-Stokes equations using an implicit, finite volume method by Thomas and Walters. Turbulent closure was achieved with the Baldwin-Lomax algebraic turbulence model. The computational grid contained approximately 9000 points. In their results they focused on the C_p distributions over the cavity surface. The C_p distributions showed reasonable agreement with the experimental evidence they collected.

Rizetta[39] simulated both a two and three dimensional cavity at Mach number 1.5 with L/D ratio of 5.07 and length-to-width (L/W) ratio of 1.90. He solved the Reynolds averaged Navier-Stokes equations using a time dependent, explicit, unsplit, two step predictor-corrector finite difference algorithm by MacCormack. Turbulence closure was achieved by the Baldwin-Lomax two layer formulation. The computational grid was a cartesian mesh with 105 x 35 x 30 points above the cavity and 74 x 29 x 20 points inside the cavity for the three dimensional case. The two dimensional simulation used the same grid minus the last dimension. Comparison of the two and three dimensional results show general agreement. However, both were less accurate at the trailing edge bulkhead compared to the experimental data of Kaufman et al[46]. The spectrums also showed that the oscillation amplitudes of both two and three dimensional simulations are larger than the experimental data, with the two dimensional being greater than the three dimensional. Frequencies calculated appear reasonably accurate, with three dimensional in better agreement than two dimensional. However, the differences are not large and the flow appears fundamentally two dimensional.

Suhs[40] investigated a three dimensional cavity both with and without a leading edge spoiler. The cavity had a L/D ratio and L/W ratio of 4.5. The Mach number was 1.2. He solved the Navier-Stokes equations using a thin layer approximation and an implicit solver using the Pulliam-Steger algorithm. Turbulence was modelled using the Baldwin-Lomax model. The grid was composed of two overlapping grids. The results include C_p distributions on cavity walls and frequency spectrums. Both C_p distributions and frequency spectrums show good agreement with experimental data from Kaufman et al[46]. The spectrums were less accurate at higher frequencies and only predicted the first two modes of cavity oscillations. Both the cavity with the spoiler and the cavity without the spoiler showed similar trends.

Shih, Hamed, and Yeuan[41] simulated a two dimensional cavity with L/D of 5.07 at a Mach number of 1.5. They solved the mass averaged Navier-Stokes equations using Beam and Warming's implicit, approximate factorization finite difference scheme. The turbulence model used was the coupled k-ε. The grid was cartesian and contained 150 x 51 points above the cavity and 96 x 40 points inside the cavity. The pressure distribution results on the cavity walls are reasonable when compared to the data of Kaufman et al.[46], though no better than Rizetta's. No spectrum analysis was performed. The trailing edge pressures were underpredicted. The authors suggested that the k-ε turbulence model might be responsible for the underprediction.

CHAPTER 3

EXPERIMENTAL APPARATUS

The experimental effort was performed in the Gas Dynamics Laboratory at the University of Tennessee Space Institute. An 8" by 8" supersonic blowdown wind tunnel was used to produce a Mach 1.75 flow over the cavity in the tunnel floor. Static and dynamic pressures were measured and Schlieren movies were taken.

Cavity

The rectangular cavity had internal dimensions of 1.5" wide by 1.5" deep by 6.5" long. It was constructed of aluminum and inset flush into the floor of the tunnel test section. The bottom of the cavity contained one static pressure port, two access ports for dynamic pressure transducers, and one access port for the traversing probe. The probe traverse port was sealed when the probe was not in use. Figure 3-1 illustrates the cavity.

Injection Apparatus

Mass was injected through perforated plates, 2.0" wide by 2.75" long, each having a varying number, size, and distribution of holes. The injection plates were located immediately upstream of the cavity and constructed from

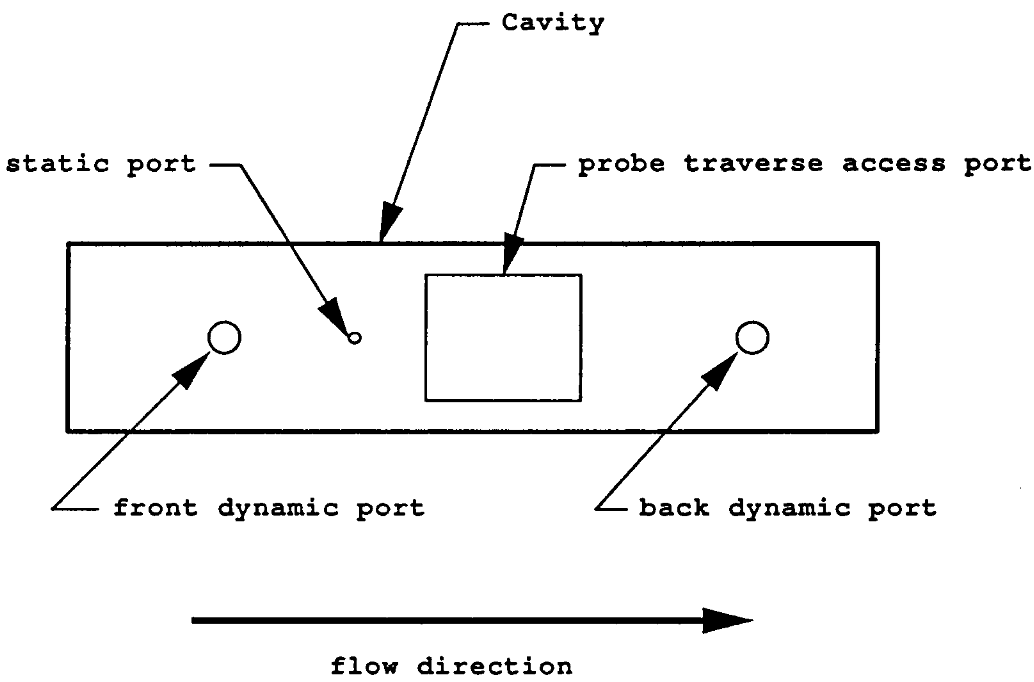

Figure 3-1 Diagram of cavity viewed from above

aluminum. The injection plate was supplied with air from a plenum located beneath, and the plenum was supplied by a two inch iron pipe from storage tanks. An orifice plate and two static ports were installed in the supply pipe to measure the mass flow rate. Figure 3-2 shows the three injection plates. Plate 2 had 90 holes with diameters of .0625 inches. Plate 9 had 190 holes with diameters of .03125 inches. The holes for Plate 9 were distributed in three streamwise rows. Plate 8 had 350 holes with diameters of .015625 inches.

Traversing Probes

Two five hole cone probes, one with a 15° half angle and one with a 30° half angle, were used in a traversing mechanism. The probes were to be used to measure flow angularity as well as mach number, but this was not successful. As a result, only the central port was used to measure the total pressure and only flow speed will be calculated. The probes were 0.070" in diameter and the five ports were 0.008" in diameter. The probes were mounted in holders which could be moved vertically during the tunnel runs. The probes were mounted in two positions inside the tunnel, a forward position where the probe tip was just at the cavity leading edge and a back position where the probe tip was just at the cavity trailing edge. One holder had a rotatable crank arm allowing it to reach two stations at both

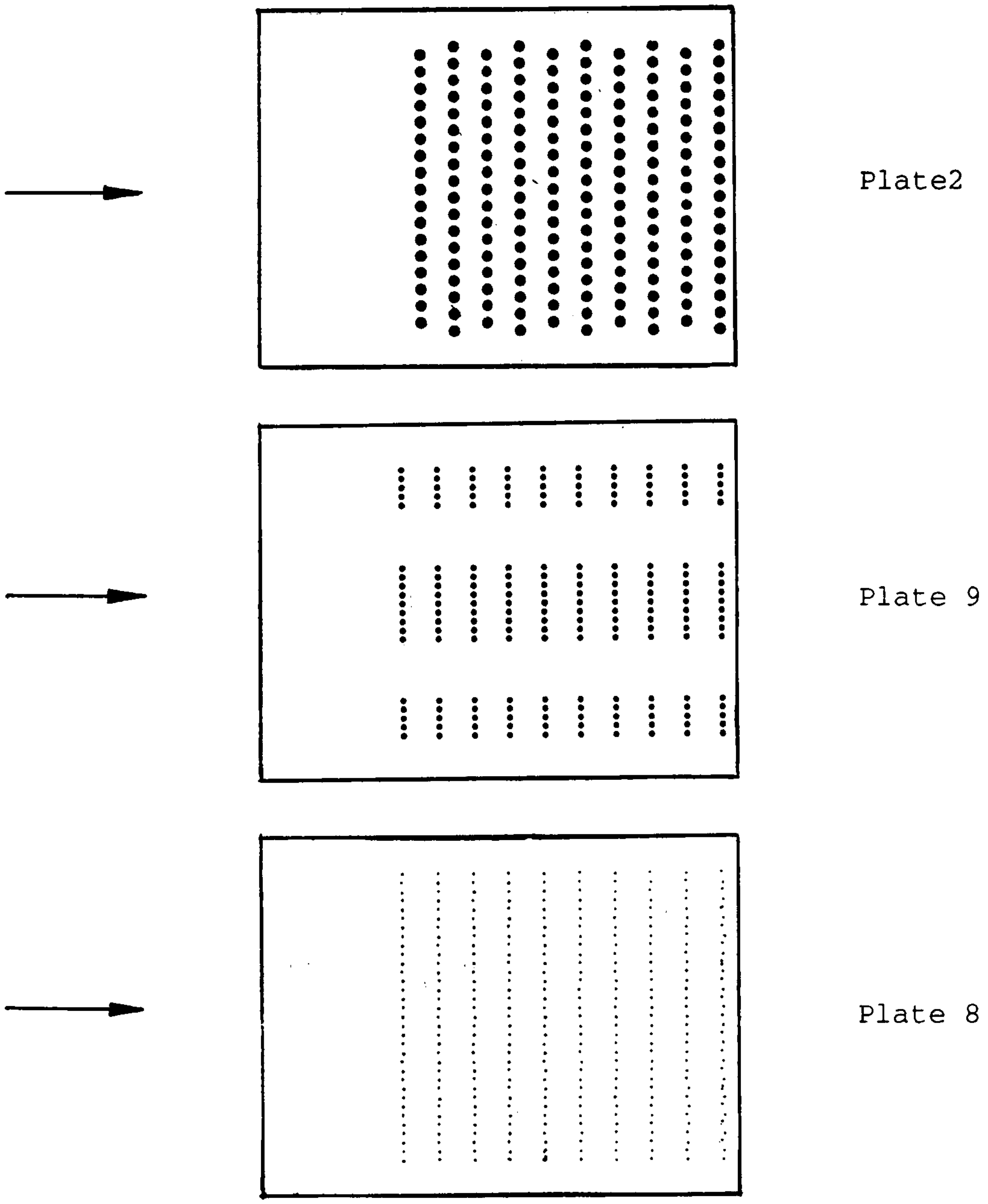

Figure 3-2 Injection plates

the front and back positions. The holders were moved by a threaded shaft connected to a stepper motor. The stepper motor was controlled during tunnel runs by a computer. Figure 3-3 shows a probe inside the tunnel at the back position. The probes were traversed at six stations near the cavity. Figure 3-4 shows the six stations.

Test Section

The test section of the wind tunnel measures 8" by 8" by 48". The injection plate and cavity are preceded by one static port on the floor centerline. The sides and roof of the test section adjacent to the injection plate and cavity are transparent and allow Schlieren videotape to be taken. The transparent sections do not extend into the cavity. Beside the cavity is a static port. Downstream of the cavity is an access port for the traversing probe. Downstream of the access port, on the tunnel centerline, are twenty four static ports located on one inch centers. Figure 3-5 illustrates the various ports and their locations.

Instrumentation

The static ports downstream of the downstream traversing probe access port were connected to a scanivalve using a Scanivalve® PDCR24 transducer. All other static ports were connected to Validyne DP15 transducers. The dynamic pressure transducers are Endevco models 8514-10 and 8510-c-15. The Validyne transducers were connected to Validyne

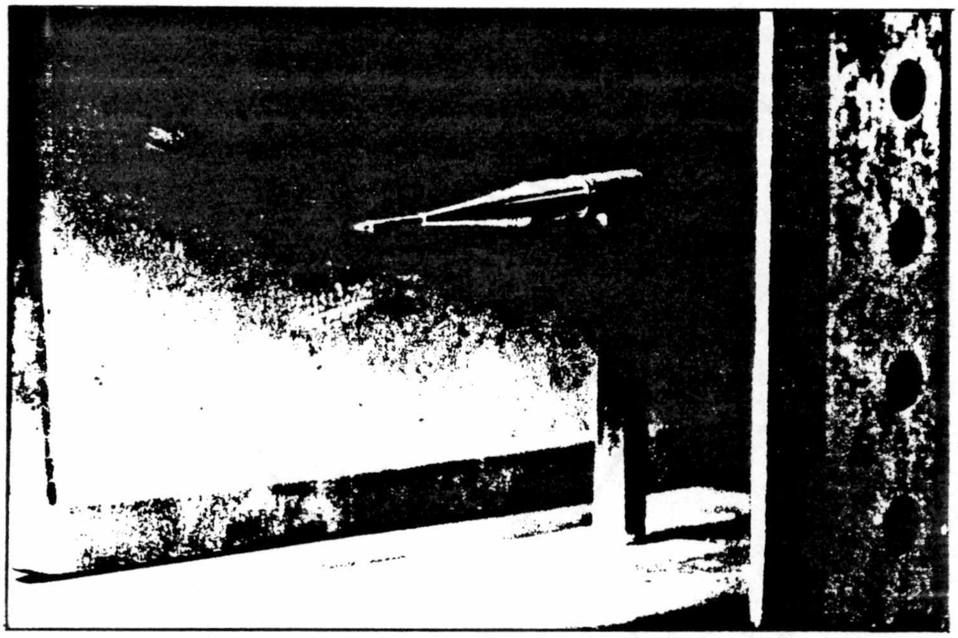

Figure 3-3 Picture of cone probe in tunnel
from Lambert[44]

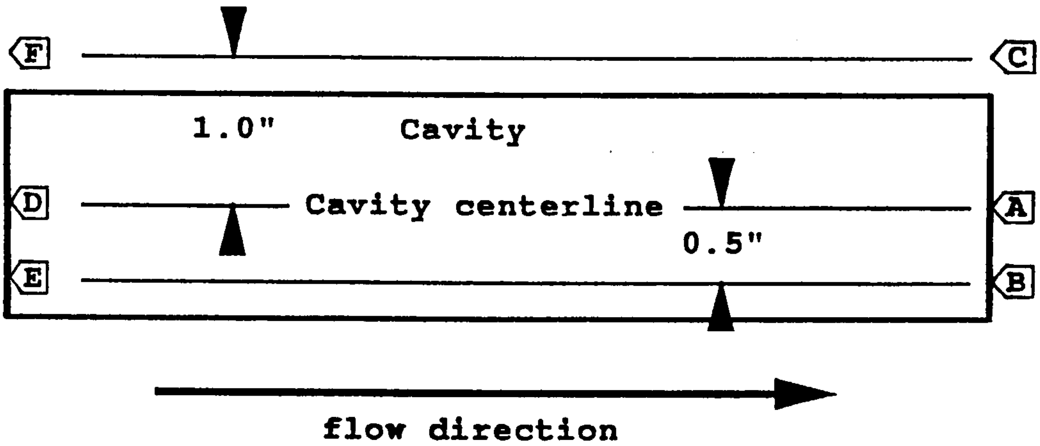

Figure 3-4 Six stations of the cone probe

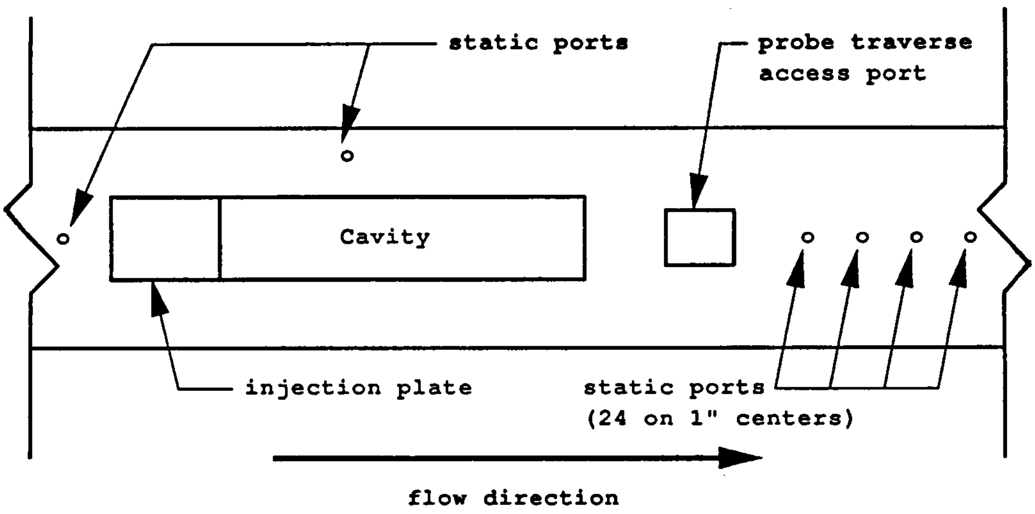

Figure 3-5 Diagram of tunnel floor viewed from above

CD19 amplifiers. The Endevco transducers used Validyne SG71 amplifiers. The amplifier outputs were connected to a analog-to-digital converter attached to a Northgate 286 IBM compatible personal computer.

The amplified dynamic pressure transducer signals were also connected to two spectrum analyzers. Each signal was routed to an HP3582A Spectrum Analyzer as well as to a 486 personal computer running Labview software. The spectrum analyzers averaged either 8 or 16 sets of data, each set containing 1024 data points collected at 10,000 data points per second.

Tunnel runs, probe movement, and data acquisition were controlled using programs run on the Northgate 286 personal computer. Both probe data and spectrum data could not be collected during the same tunnel run.

Flow Conditions

The tunnel was run at a nominal Mach number of 1.75 and Reynolds number of 17 million per foot.

Experimental Procedures

The procedures used in collecting data were generally similar for both the collection of dynamic pressure data and the cone probe traverses. All runs start by zeroing the transducer amplifiers and adjusting the schlieren when it was used. The tunnel was started by the tunnel operator, and the nominal flow mach number was established. When dynamic pressure data was measured the spectrum analyzers were triggered by one person at a signal from the tunnel operator who also triggered the data collection program and controlled the mass injection rate. When the cone probe was traversed the tunnel operator triggered a different data collection program which also controlled the probe traversing mechanism. A second person was generally used to control the mass injection rate during probe traverse runs. The probe traverses were slowed by the need to park the probe at each point for over a second to allow the system to come to equilibrium. The parking time was required due to the small diameter of the flow passages inside the cone probe and in the connecting tubing. Tunnel runs took an average of 23 seconds.

CHAPTER 4

COMPUTATIONAL APPARATUS

Code

The computer program used for the computational work was the NPARC code. NPARC was developed for use in the Engine Test Facility at the Arnold Engineering Development Center[42]. NPARC was derived from the ARC codes developed by Pulliam[42]. NPARC has two versions, NPARC2D is used in two dimensional cases, and NPARC3D is used for three dimensional cases.

NPARC is based on the conservation law form of the complete Navier-Stokes equations[42]. Specifically, the nondimensional general curvilinear coordinate form of the Navier-Stokes equations are used. (Note: The following equations make use of the Einstein summation convention for the sake of brevity.) They are as follows:

$$\frac{\partial \hat{Q}}{\partial t} + \frac{\partial \hat{F}_j}{\partial \xi_j} = \frac{1}{Re}\frac{\partial \hat{G}_j}{\partial \xi_j}$$

where the vectors involved are,

$$\hat{Q} = \frac{1}{J}\begin{bmatrix} \rho \\ \rho u_i \\ E \end{bmatrix}$$

$$\hat{F}_j = \frac{1}{J}\begin{bmatrix} \rho U_j \\ \rho u_i U_j + P\dfrac{\partial \xi_j}{\partial X_i} \\ (E+P)\,U_j - P\dfrac{\partial \xi_j}{\partial t} \end{bmatrix}$$

$$\hat{G}_j = \frac{1}{J}\begin{bmatrix} 0 \\ \hat{\tau}_{ij} \\ u_k \hat{\tau}_{jk} - \hat{q}_j \end{bmatrix}$$

and the contravariant velocities, transformed viscous stress tensor, and transformed heat flux vector are,

$$U_j = \frac{\partial \xi_j}{\partial t} + u_k \frac{\partial \xi_j}{\partial X_k}$$

$$\hat{\tau}_{ij} = \frac{\partial \xi_j}{\partial X_k} \tau_{ik}$$

$$\hat{q}_j = \frac{\partial \xi_j}{\partial X_k} q_k$$

finally, the viscous stress tensor, heat flux vector, velocity and temperature derivatives are,

$$\tau_{ij} = \mu \left(\frac{\partial u_i}{\partial X_j} + \frac{\partial u_j}{\partial X_i} \right) + \lambda \frac{\partial u_k}{\partial X_k} \delta_{ij}$$

$$q_j = -\frac{K}{\beta_r Pr} \frac{\partial T}{\partial X_j}$$

$$\frac{\partial u_i}{\partial X_j} = \frac{\partial \xi_k}{\partial X_j} \frac{\partial u_i}{\partial \xi_k}$$

$$\frac{\partial T}{\partial X_j} = \frac{\partial \xi_k}{\partial X_j} \frac{\partial T}{\partial \xi_k}$$

NPARC is also based on the assumption of a thermally and calorically perfect gas, the Stokes hypothesis, the Sutherland viscosity law, and a constant Prandtl number.

The turbulence model is an algebraic model based on the Thomas formulation of the Baldwin and Lomax model. When the flow is turbulent, the viscous coefficients are calculated by:

$$\mu_{total} = \mu + \mu_T$$

$$K_{total} = K + \mu_T \frac{Pr}{Pr_T}$$

The turbulent viscosity is found as follows:

$$\mu_T = Re \; \rho \; \omega \; l^2$$

where ω is the vorticity, ρ is the density, Re is the Reynolds number, and the mixing length, l, is:

$$l = \frac{l_o}{\omega_c} [Max(|u_j|) - Min(|u_j|)]$$

when the flow is unbounded. However, when the flow is bounded, the mixing length, l, becomes:

$$l = l_o d(1 - e^{-\frac{d^+}{A^+}})$$

where

$$d = \sqrt{(X-X_w)^2 + (Y-Y_w)^2 + (Z-Z_w)^2}$$

$$d^+ = \sqrt{\frac{Re\ \rho_2\ \omega\ d^2}{\mu_w}}$$

and l_o is the von Kármán constant, A^+ is the van Driest constant, ω_c is the value of the vorticity at the point where $|\omega_j|$ is a maximum, and all variables with a subscript w are evaluated at the wall.

NPARC has several options for solving the matrices resulting from the finite differencing of the equations. The Beam and Warming approximate factorization scheme is primarily used for finding the steady state solution. The alternate solver is used for time-dependent flows. This solver is a three, four, or five stage Runge-Kutta solver developed by Jamison. The four stage Runge-Kutta solver was chosen for the cavity flow simulation.

Computational Grid

The grid used in the simulation is cartesian with both uniform and non-uniform spacing. The grid is bounded by the cavity surfaces, upstream and downstream surfaces, upstream flow inlet, downstream flow outlet, and the upper surface. The upper surface represents the tunnel ceiling over the cavity. The dimensions of the grid surfaces match the dimensions of the experimental cavity and tunnel. Several non-uniform spacings were tried. A hybrid scheme was developed which used stretched sine distributions on all solid surfaces with two exceptions. The surfaces upstream and downstream of the cavity used a uniform spacing with the smallest grid dimension , which was 0.02 inches. This spacing provided better resolution of the critical shear layer area. The grid had dimensions of 117 x 121 points. Some of the grid points were not used in the computation as the boundary geometry left them outside the flow. Figure 4-1 shows the grid. Figure 4-2 shows those points used in the computation. (Note: Every other point has been removed for reasons of clarity.)

Boundary Conditions

All solid surfaces had the no slip condition enforced. The inlet flow, on the left side, was frozen to a velocity profile set at program initiation that reflected the freestream Mach number and boundary layers at both the top and bottom following the 1/7 power law. The outflow, on the right, was defined by specifying the outflow static pressure.

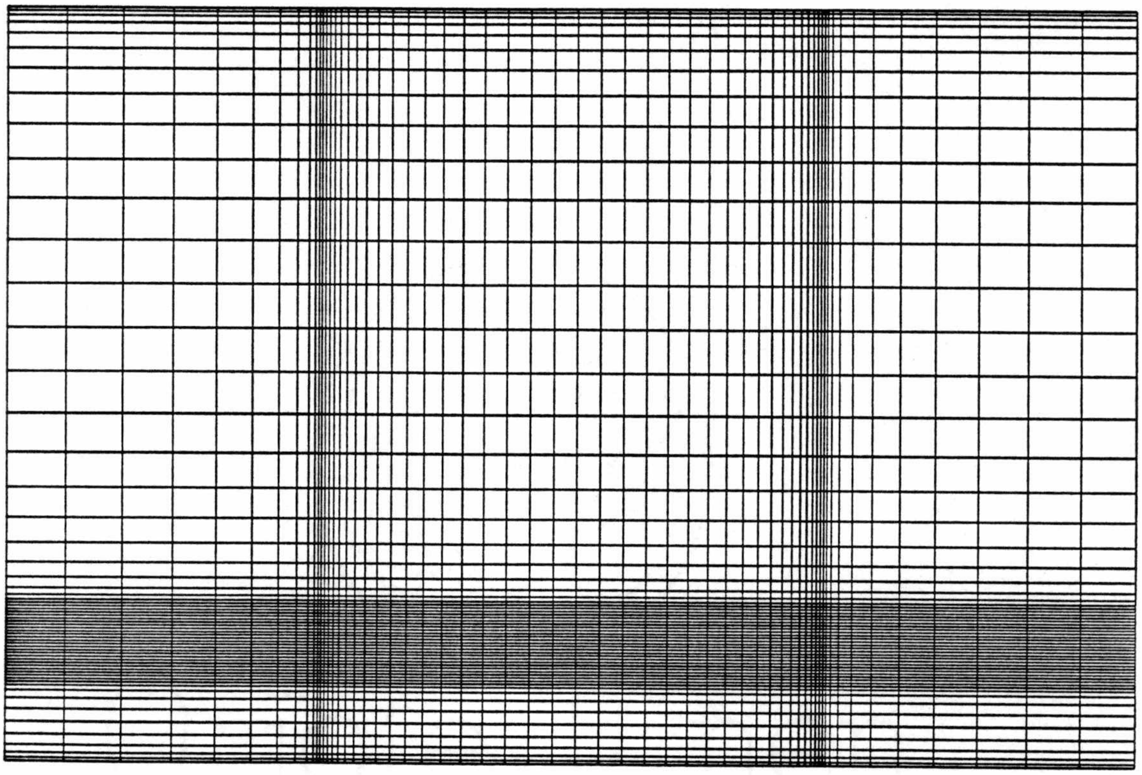

Figure 4-1 Computational grid

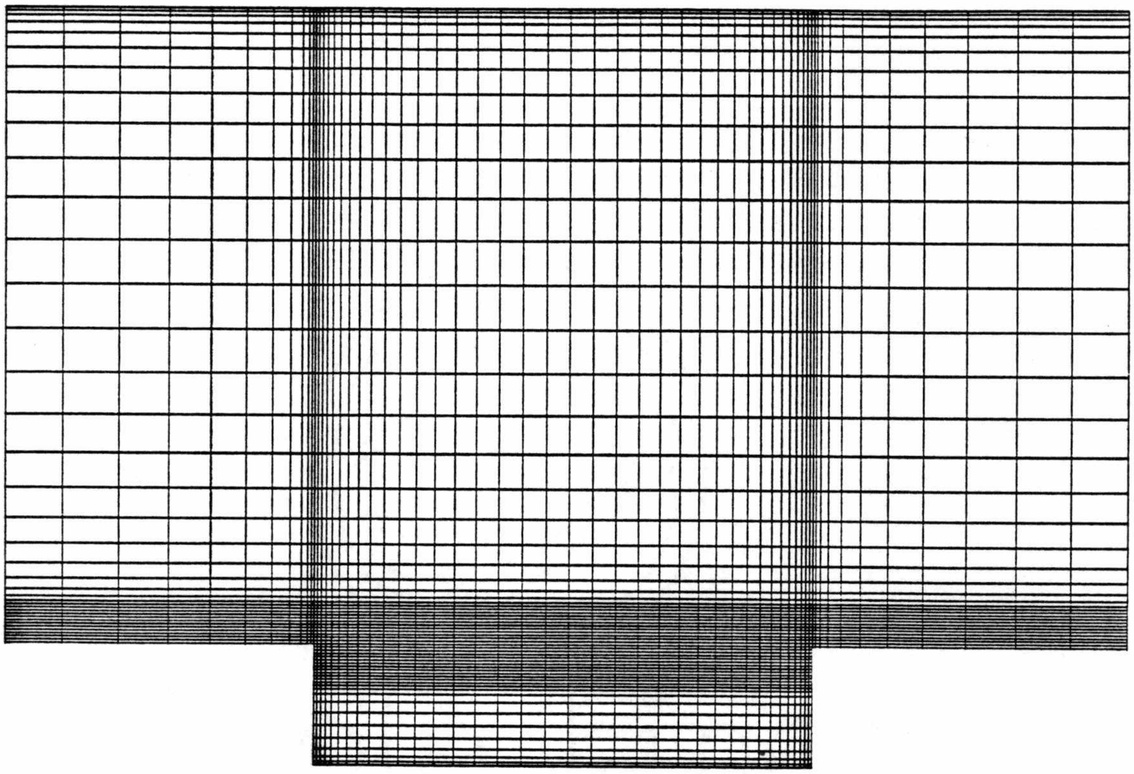

Figure 4-2 Computational grid showing points used

Hardware

The computer hardware used for the computational simulation was a Silicon Graphics Iris Indigo using a single R4000 processor operating at 100/50 megahertz. The memory capacity was 80 megabytes and the hard drive capacity was 1342 megabytes.

CHAPTER 5

RESULTS

Experimental Results

The results of the experimental effort may be divided into two areas. The first area involves the spectrum data for three injection plates at different mass injection rates. The second area involves the velocity profiles for a single plate at different mass injection rates and cone probe positions.

Figures 5-1 through 5-4 are spectrums resulting from the cavity flow with injection through plate 8. The horizontal scale is the frequency in hertz and the vertical scale is the amplitude in decibel volts (dBV). A decibel volt equals 20 times the base ten log of a voltage. Each figure shows two spectrums. Channel 1 is for the dynamic pressure transducer located at the front of the cavity, channel 0 is for the dynamic pressure transducer at the back of the cavity. The header information for each figure contains the frequency and amplitude of the peak for each channel. Table 5-1 contains spectrum results for injection plates 9, 2, and 8. The table contains the peak amplitude at the back dynamic pressure transducer port in decibel volts (dBV), pounds per square inch (psi), and sound pressure level (SPL). The table also contains the blowing parameter B, and two derived

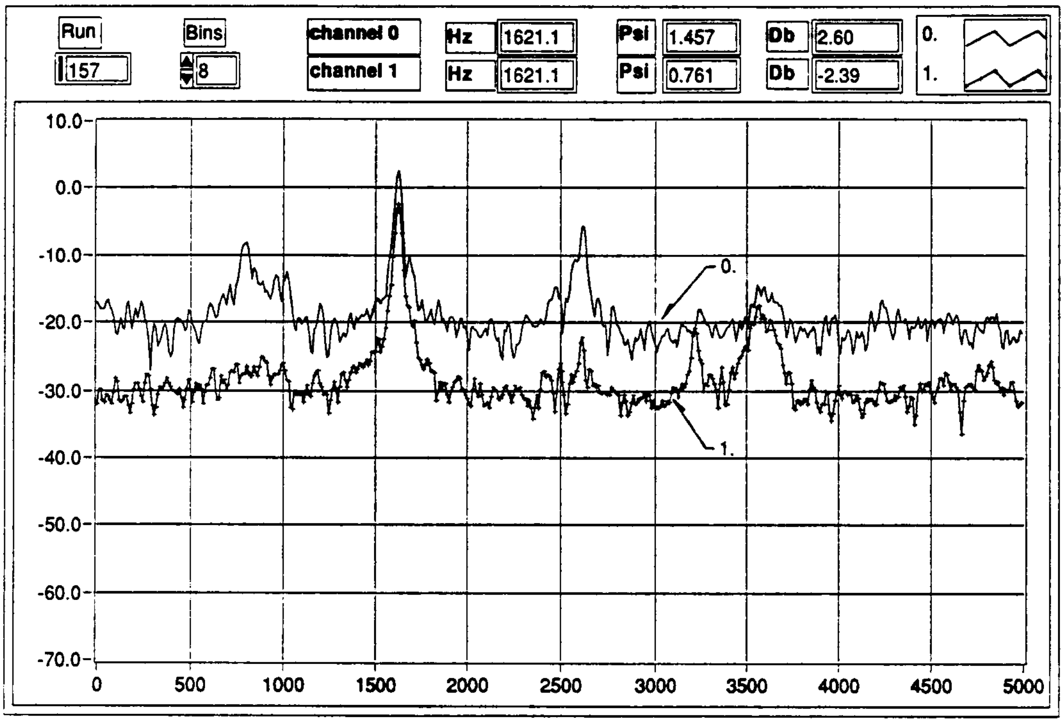

Figure 5-1 Spectrum results for no injection

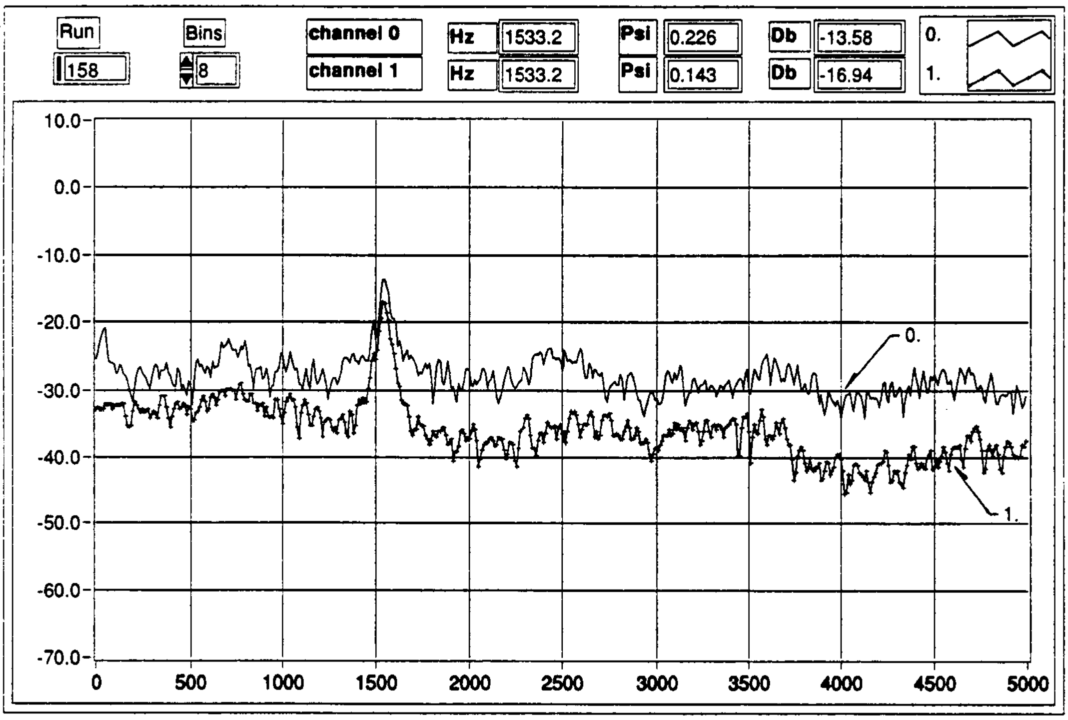

Figure 5-2 Spectrum results for injection of 0.03 lbm/s

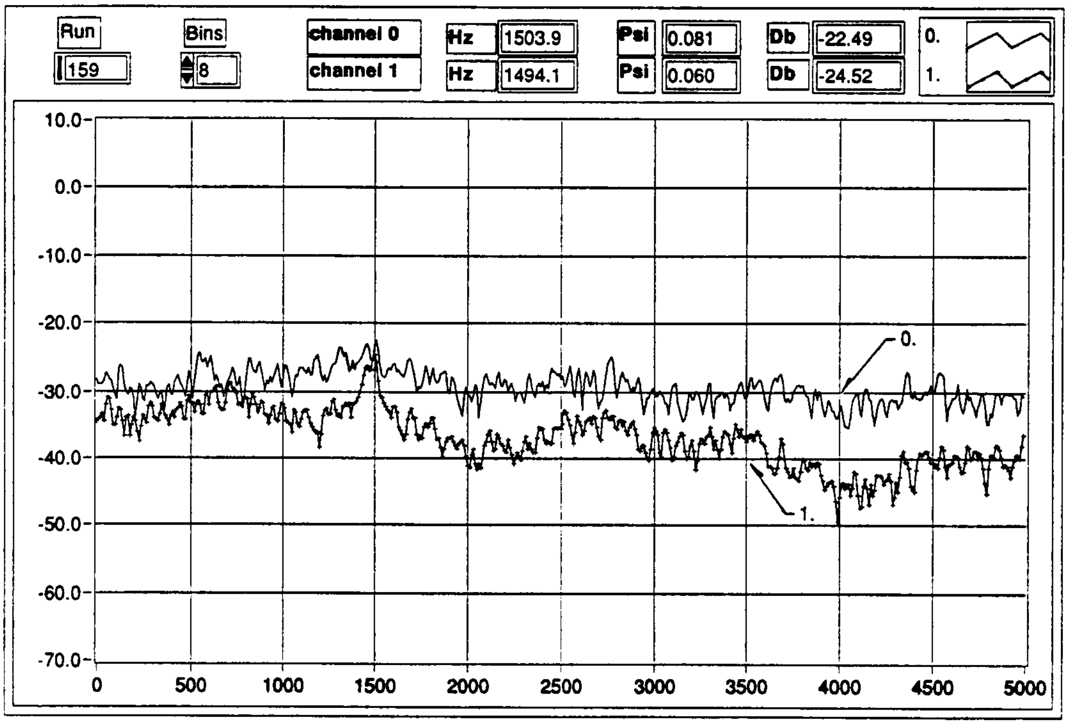

Figure 5-3 Spectrum results for injection of 0.05 lbm/s

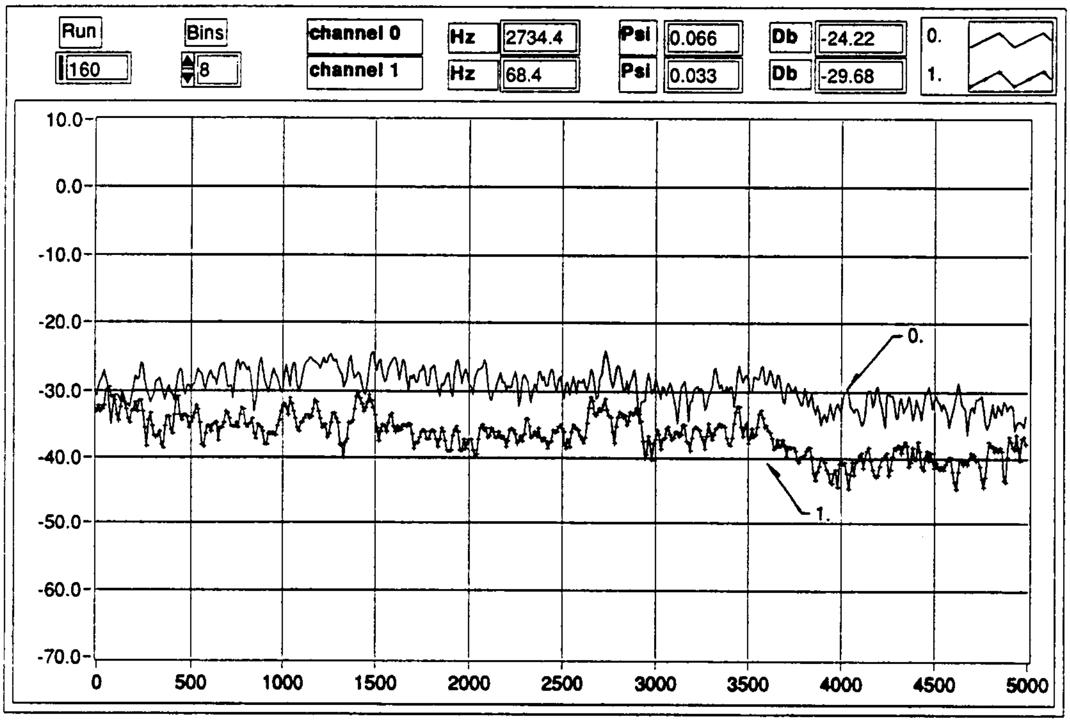

Figure 5-4 Spectrum results for injection of 0.10 lbm/s

Table 5-1 Cavity oscillation reduction results

Plate	Run	$\frac{P_{inj}}{P_s}$	mass flow (lbm/s)	Peak (dBV)	Amplitudes (Psi)	(SPL)	B	B_c ($X10^3$)	B_d ($X10^3$)
2	152	*	0.00	3.61	1.64	175	0.00	0.00	0.00
2	153	1.17	0.03	-2.58	0.80	169	0.18	5.09	16.3
2	154	1.39	0.05	-9.26	0.37	162	0.30	8.49	27.2
2	155	2.25	0.10	-24.58	0.06	146	0.62	17.5	56.0
9	113	*	0.00	5.18	1.93	176	0.00	0.00	0.00
9	114	1.82	0.05	-18.34	0.13	153	0.48	7.18	22.9
9	115	2.32	0.10	-20.36	0.10	151	0.95	14.2	45.4
9	116	3.17	0.15	-19.14	0.12	152	1.41	21.1	67.5
8	157	*	0.00	2.60	1.46	174	0.00	0.00	0.00
8	158	2.63	0.03	-13.58	0.23	158	0.78	5.37	17.2
8	159	4.43	0.05	-22.49	0.08	149	1.29	8.87	28.4
8	160	8.85	0.10	-24.22	0.07	148	2.69	18.5	59.2

* not applicable if no injection

$$B = \frac{\rho_{inj} u_{inj}}{\rho_\infty u_\infty}$$

$$B_c = B \cdot \frac{A_{inj}}{A_{cav}}$$

$$B_d = B \cdot \frac{A_{inj}}{A_{pinj}}$$

parameters, B_c, which equals B multiplied by the ratio of the injection area to the cavity floor area, and B_d, which equals B multiplied by the ratio of the injection area to the area contained within the perimeter of a rectangle which just circumscribes all the injection holes. The almost complete suppression of the peak pressure oscillations as well as a reduction in the broadband fluctuations is apparent from the table and figures.

Figure 5-5 is a graph of the amplitude reduction resulting from mass injection versus the mass injection rate for all three plates. The no mass injection amplitudes are used as the reference. The errorbars are +/- 2 dBV and were the repeatability observed during 12 consecutive runs without mass injection. The figure demonstrates the diminishing returns for mass injection above 0.05 lbm/s. Plate 8 appears to suppress the cavity oscillations best.

Figure 5-6 graphs the amplitude reduction versus the injection area of the plates for three mass injection rates. Lower injection areas provide improvement in amplitude reduction, although when the injection area is zero the reduction must also be zero. Figures 5-5 and 5-6 may suggest that greater injection uniformity produces better suppression characteristics.

Figures 5-7 through 5-12 are velocity profiles derived from pressure data collected by the cone probe traverses. The data was collected at six stations and three mass

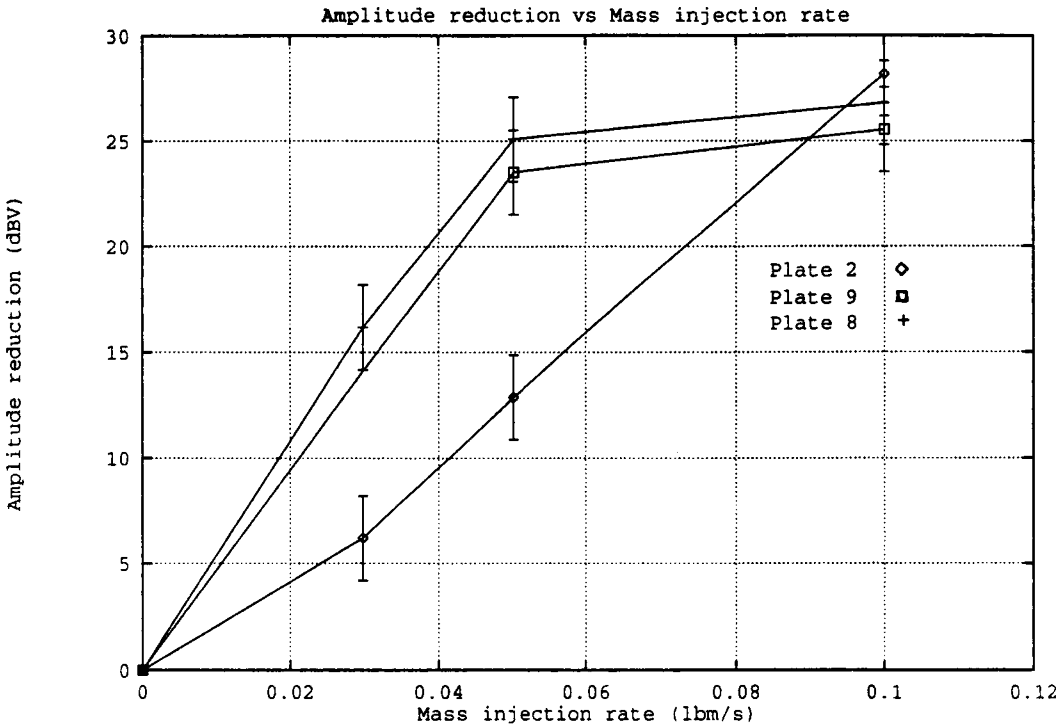

Figure 5-5 Amplitude reduction vs Mass injection rate

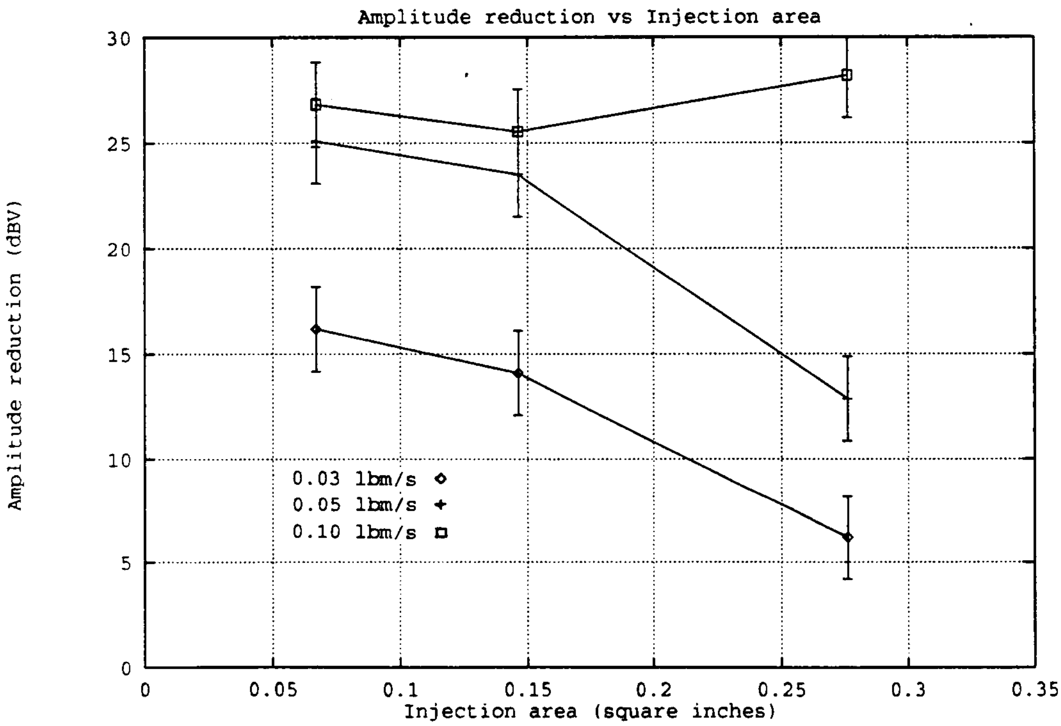

Figure 5-6 Amplitude reduction vs Injection area

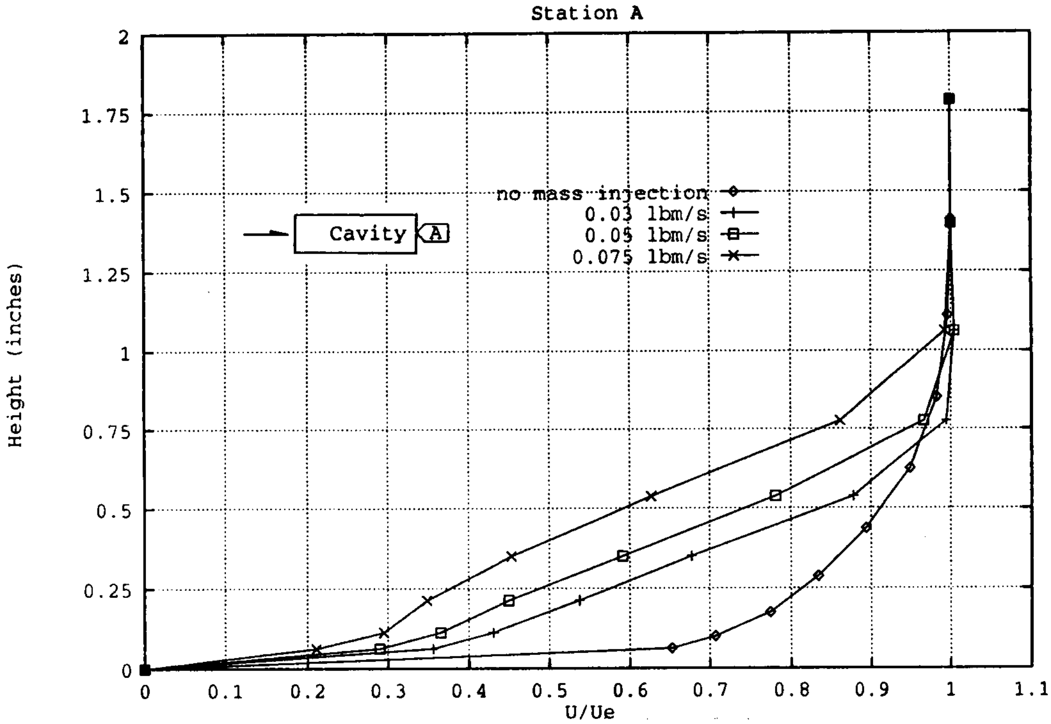

Figure 5-7 Velocity profiles at station A

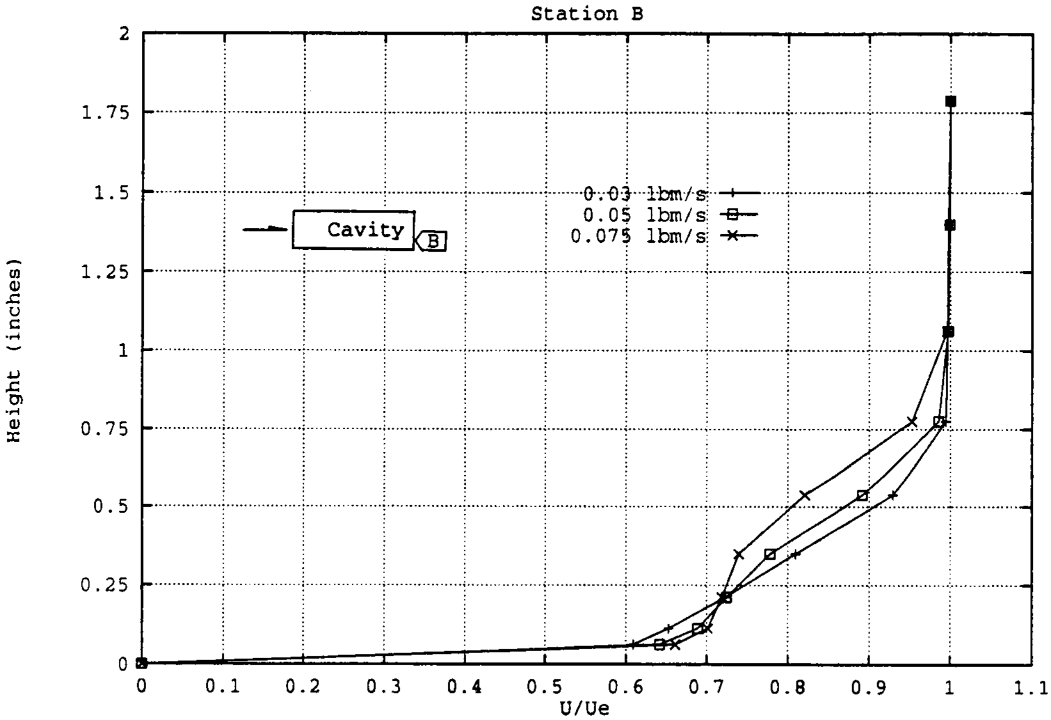

Figure 5-8 Velocity profiles at station B

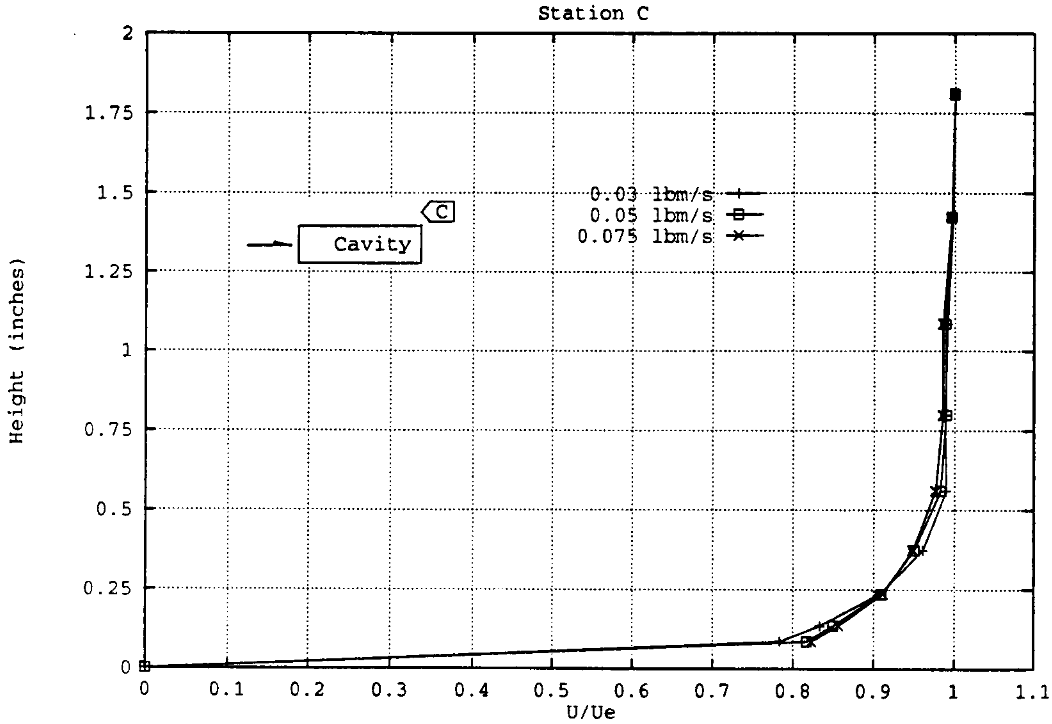

Figure 5-9 Velocity profiles at station C

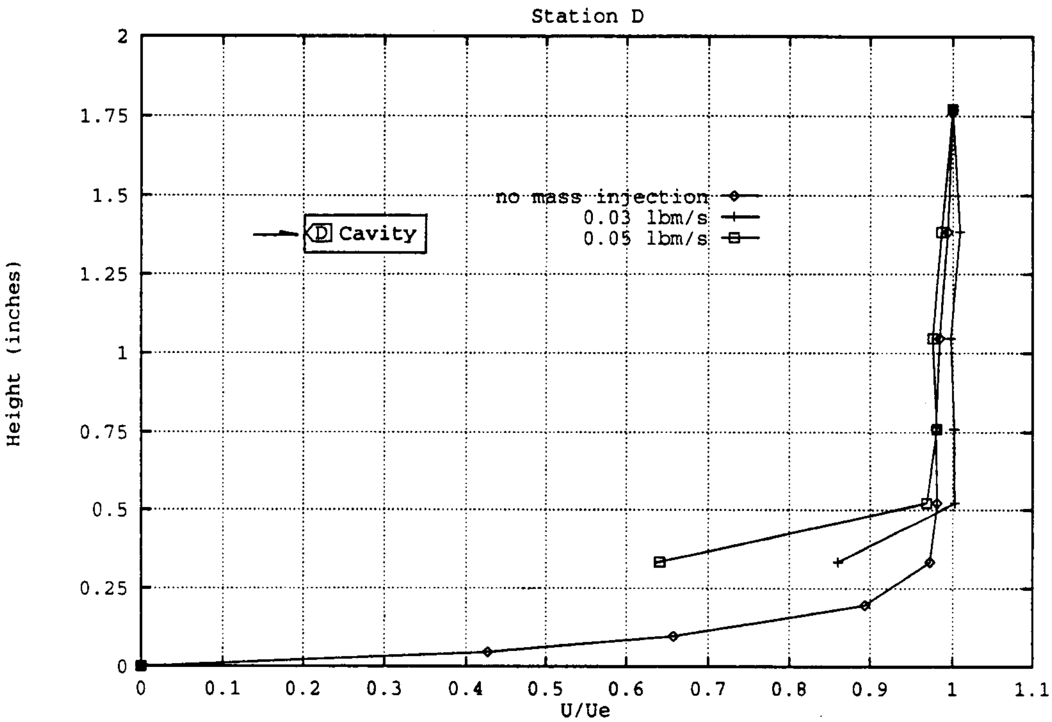

Figure 5-10 Velocity profiles at station D

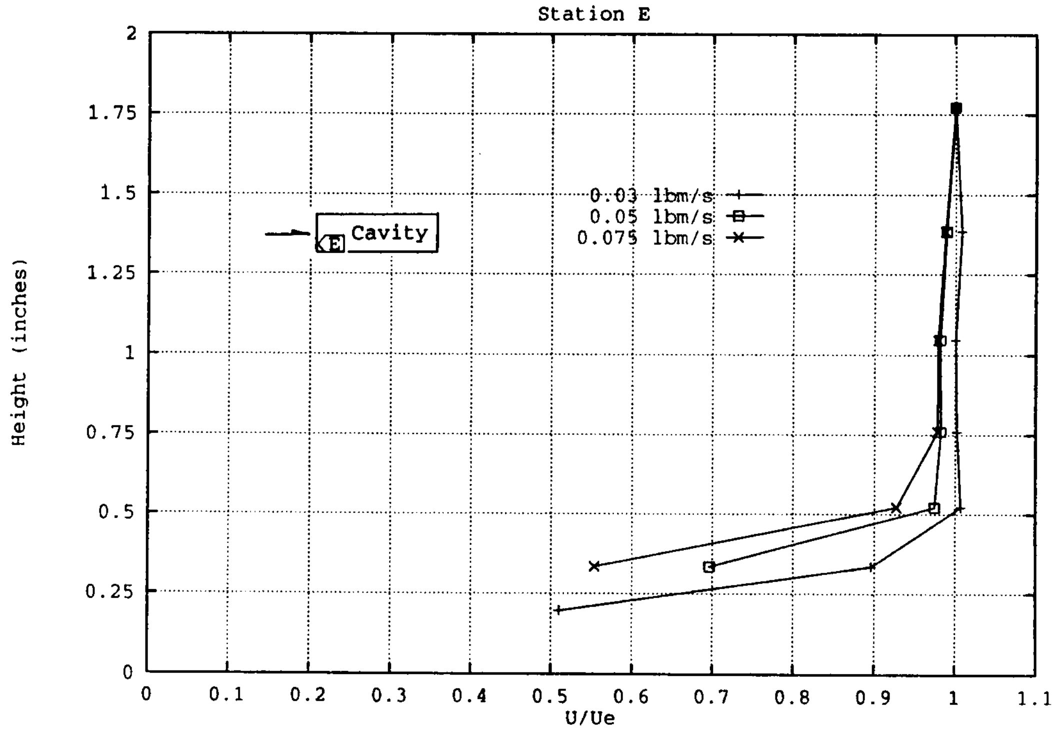

Figure 5-11 Velocity profiles at station E

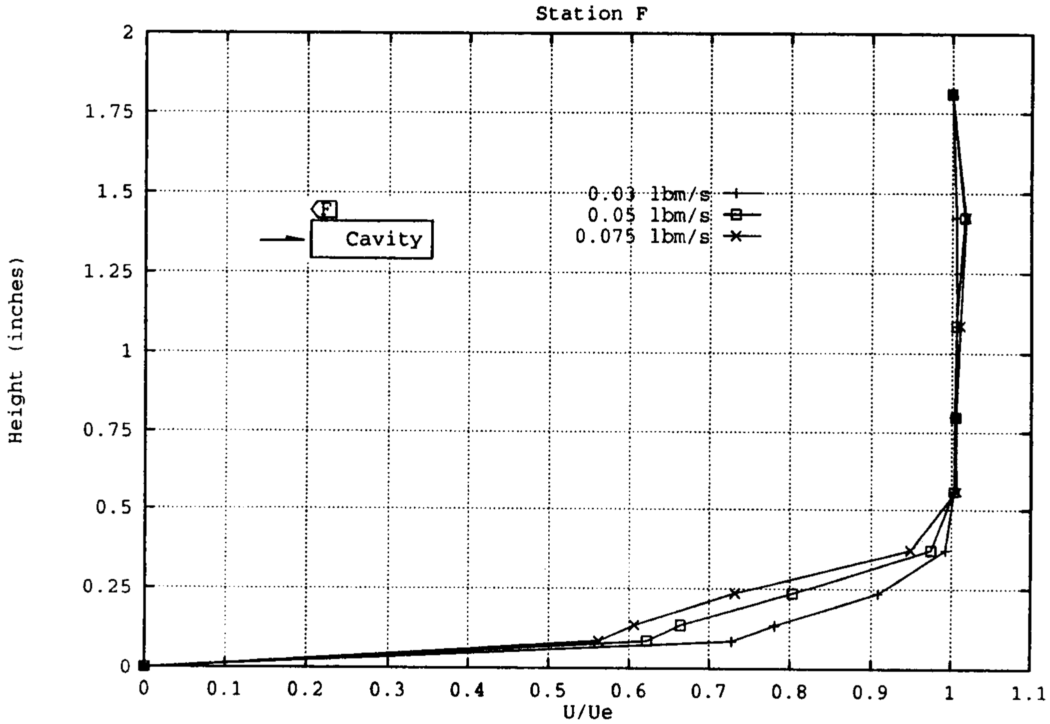

Figure 5-12 Velocity profiles at station F

injection rates with injection through plate 8. The profiles from stations D and E (as shown in figure 3-4) had to be truncated and the highest mass injection rate for station D is absent. The highest injection rate data for station D could not be reduced. The data for stations D and E showed that some lower profile points had probe total pressures lower than the freestream static pressures and these points are not shown. A possible explanation for this might be entrainment of the boundary layer by the discrete jets and/or off angle flow approaching the probe. The profiles show significant changes as mass injection is increased, with the changes largely restricted to the region directly behind the injection plate. Inflections points in the profiles appear and move upward as the mass injection rate increases. The boundary layer thickness also increases but this is less pronounced than the profile changes.

Computational Results

Initially, the computer code was run using the turbulence model in a thin layer approximation. The thin layer turbulent simulation resulted in the elimination of the shear layer motion and the pressure fluctuations. Different grids and full turbulence did not solve the problem. However, the elimination of the turbulence model did allow the free shear layer to continue oscillating. Consequently, the code was run without a turbulence model, although it was fully viscous. The flow conditions for the simulation were based on data taken during the experimental effort. The inflow Mach number was set at 1.75 and the outflow static pressure was set at 6.5 psi.

The computational results are shown in figures 5-13 through 5-17 and were produced using the FAST graphics software program. The figures are for an elapsed time of 0.0388 seconds. Figure 5-13 shows a typical density contour plot of the solution. The lateral movement of the shear layer is obvious. Figure 5-14 shows a typical velocity magnitude contour plot for the same solution. The chevron shaped contour on the left shows that the fixed inflow boundary condition does create some mismatch with the flow. Figure 5-15 shows a plot of the velocity vectors in the cavity region and for the same solution. The vectors also show the shear layer movement. Figure 5-16 is a pressure versus time plot of the wall pressure on the cavity bottom near the rear of the cavity. The amplitude swings from around four psia to around eleven psia. Figure 5-17 is a spectrum analysis of the pressure data plotted in figure 5-16. The spectrum shows only random behavior.

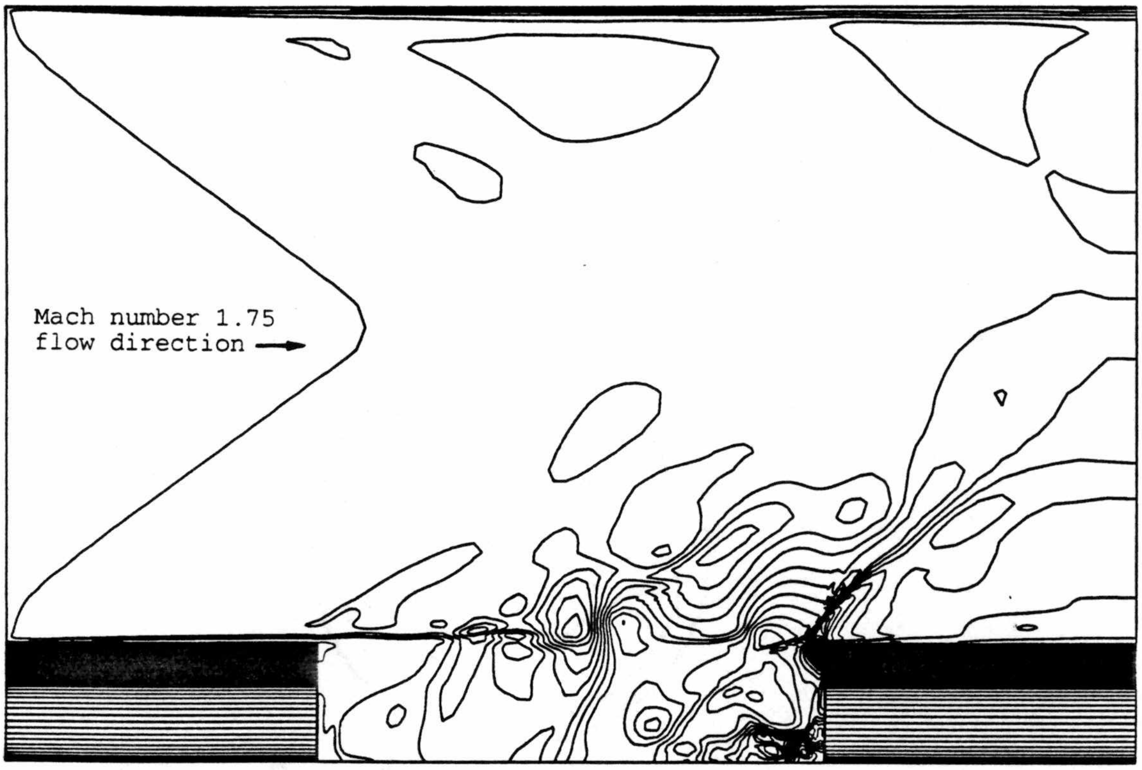

Figure 5-13 Density contour

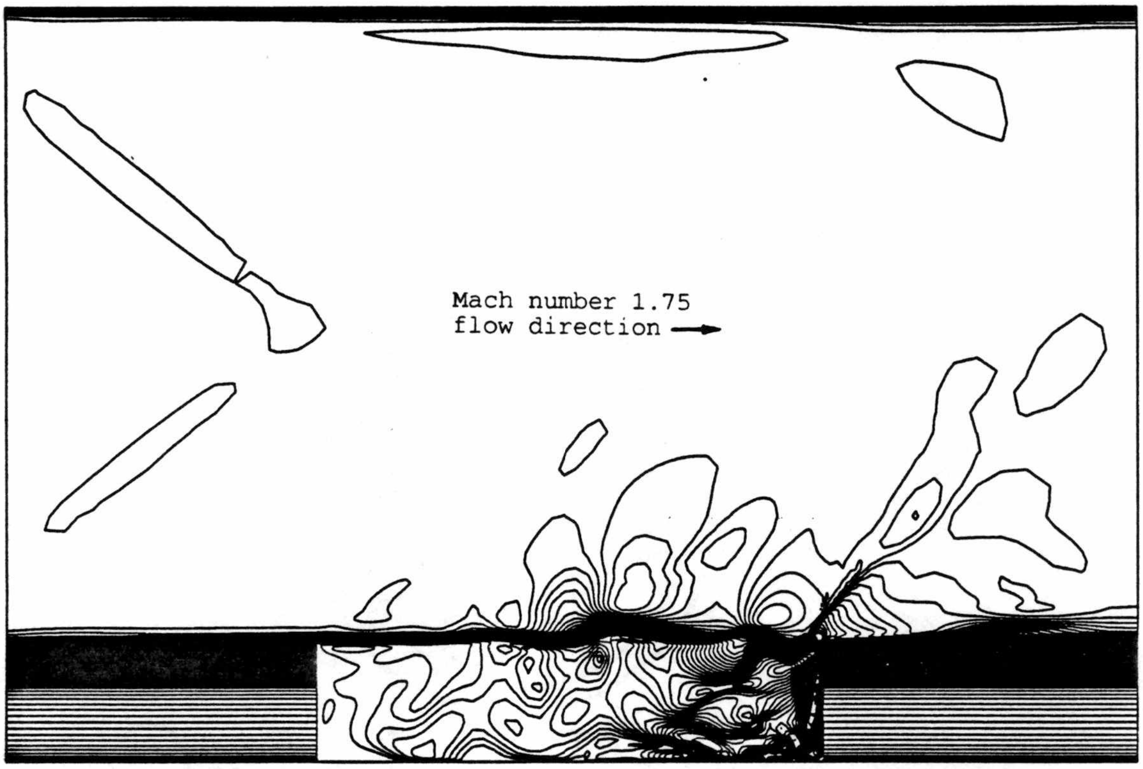

Figure 5-14 Velocity magnitude contour

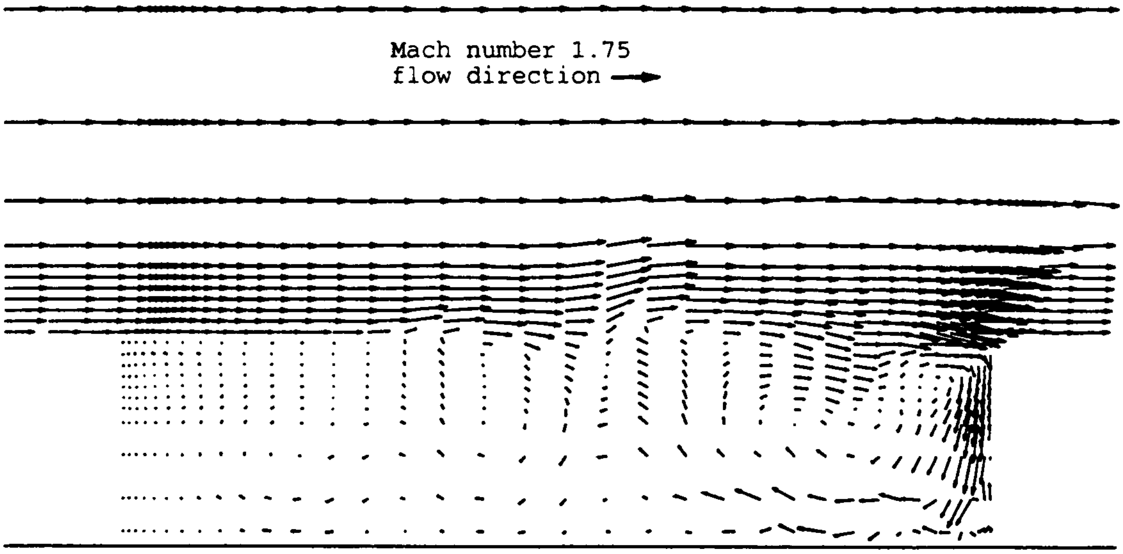

Figure 5-15 Velocity vectors in near cavity region

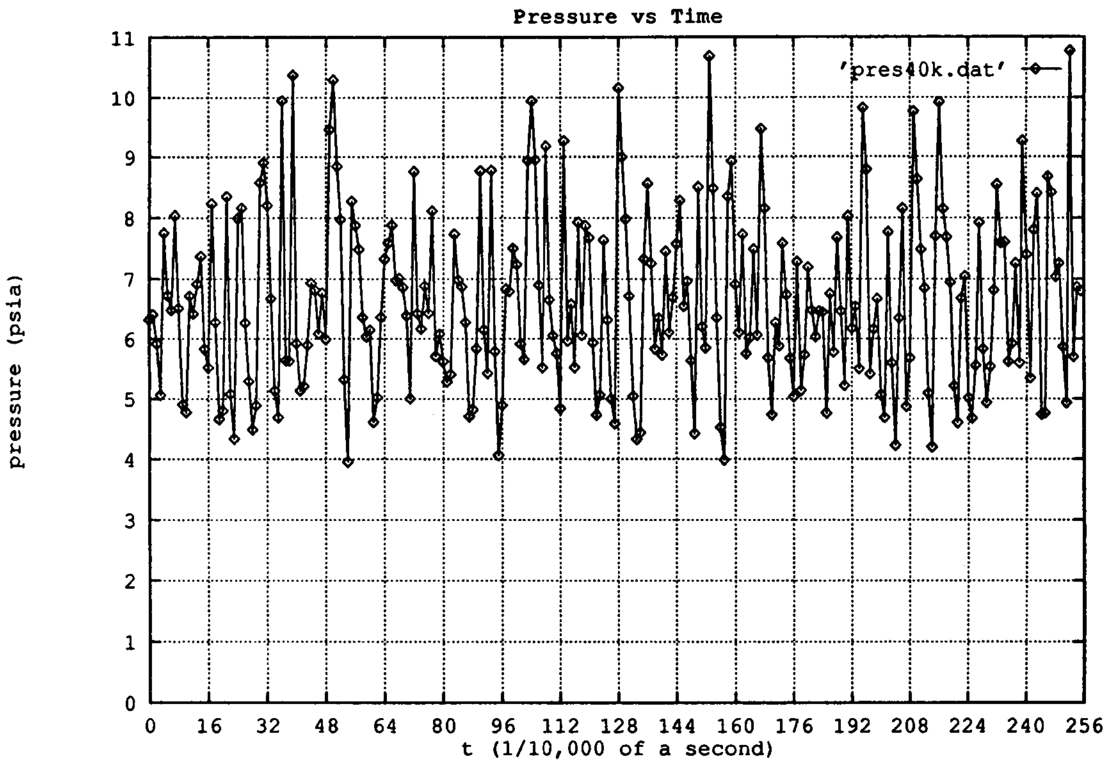

Figure 5-16 Pressure vs time on cavity bottom

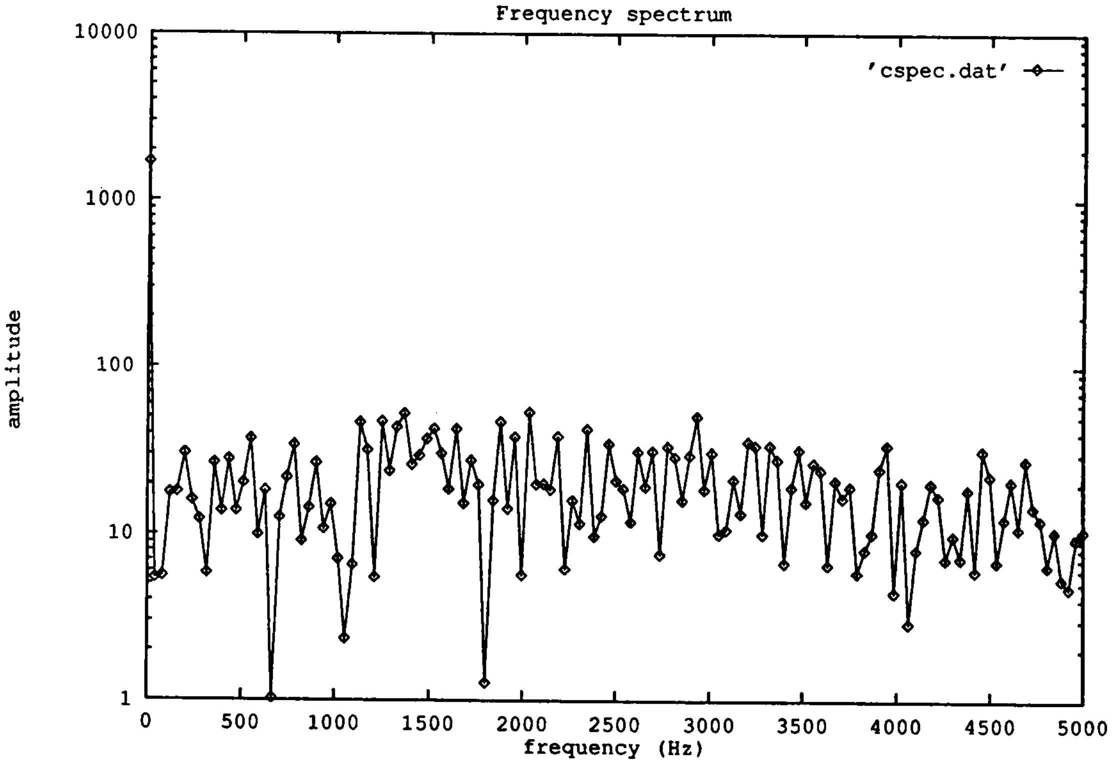

Figure 5-17 Spectrum of pressure vs time data from cavity bottom

CHAPTER 6

CONCLUSIONS AND RECOMMENDATIONS

Conclusions

The effectiveness of mass injection in suppressing cavity oscillations is directly related to the amount of mass injected. However, the greatest incremental improvements in suppression effectiveness come at the lower mass injection rates. Finally, the reduction in broadband as well as peak amplitudes demonstrates a reduction in the energy contained in the fluctuations, not a redistribution of the energy from a few frequencies to many frequencies.

The velocity profiles demonstrate that mass injection has significant effects on the flow downstream from the injection area. The loss of the lower probe traverse data points at the front of the cavity at stations D and E make conclusions about the specific effects of mass injection difficult to make. Unfortunately, the profiles from the back of the cavity reflect many effects, not just mass injection, and thus conclusions based on these profiles are also difficult. However, the upper portions of the profiles seem to indicate that boundary layer thickness is most affected at higher mass flow rates. Remembering that mass injection produces most of its effectiveness in suppression at low mass flow rates suggests either that the effect of boundary layer thickness is non-linear or that some other boundary layer parameter is of primary importance. The obvious candidate for the relevant boundary layer parameter would be the velocity profile or derivative parameters such as momentum thickness. This supports the earlier work of Vakili et al.[28] who had theorized that injection changes the stability of the shear layer through changes in the separating boundary layer and its derivative parameters.

Recommendations

The first recommendation is to redesign the mass injection apparatus. The present system is too difficult and time consuming to ensure low leakage rates. The second recommendation is to find some way of improving the number of data points acquired during probe traverse runs. Either improving the time response of the system, increasing the traverse speed, or finding a way to adjust the data so as to allow shorter parking times.

The third recommendation is to investigate more uniform injection and find a method of measuring velocity profiles at the cavity front. The final recommendation is to continue the work on the computational cavity simulation effort. A successful computational simulation capability would allow the investigation of the effects of differing upstream boundary layer parameters on cavity oscillations.

LIST OF REFERENCES

LIST OF REFERENCES

[1] Gibson, J.S., "Non Engine Aerodynamic Noise Investigation of a Large Aircraft", NASA CR 2378, October 1973

[2] Bliss, D.B. and Hayden, R.E., "Landing Gear and Cavity Noise Prediction", NASA CR 2714, July 1976

[3] Parthasarathy, S.P., Cho, Y.I., and Back, L.H., "Aerodynamic Sound Generation Induced By Flow Over Small Cylindrical Cavities", AIAA Paper No. 84-2258, October 1984

[4] Parthasarathy, S.P., Cho, Y.I., and Back, L.H., "High Intensity Tone Generation by Axisymmetric Ring Cavities on Training Projectiles", AIAA Paper No. 84-2259, October 1984

[5] Mabey, D.G., "Resonance Frequencies of Ventilated Wind Tunnels", AIAA Journal, Vol.18, No.1, January 1980, pp. 7-8

[6] Bliss, D.B., "Aerodynamic Behavior of a Slender Slot in a Wind Tunnel Wall", AIAA Journal, Vol.20, No.9, September 1982, pp. 1244-1252

[7] Shen, P., "Supersonic Flow over a Deep Cavity for a Laser Application", AIAA Journal, Vol.17, No.2, February 1979, pp.216-219

[8] Buell, D.A., "An Experimental Investigation of the Airflow Over a Cavity with Antiresonance Devices", NASA TN D-6205, 1971

[9] Tanner, C.S., "Shuttle Cargo Bay Vent Noise and its effects on Generic Payload Specifications and Testing Methods", AIAA Paper No. 84-2352, October 1984

[10] Norton, D.A., "Investigation of B47 Bomb Bay Buffet", Boeing Airplane Company, Document No. D12675, May 1952

[11] Goldman, R.L., Morkovin, M.V., and Schumacher, R.N., "Unsteady Control Surface Loads of Lifting Reentry Vehicles at Very High Speeds", AIAA Journal, Vol.6, No.1, January 1968, pp.44-50

[12] Krishnamurty, K., "Acoustic Radiation from Two-Dimensional Rectangular Cutouts in Aerodynamic Surfaces", NACA TN 3487, August 1955

[13] Roshko, A., "Some Measurements of Flow in a Rectangular Cutout", NACA TN 3488, August 1955

[14] Avidor, J.M., "Improved Free Vortex, Subsonic Aerodynamic Window", AIAA Journal, Vol.17, No.2, November 1979, pp.216-219

[15] Rockwell, D., "Oscillation of Impinging Shear Layers", AIAA Journal, Vol.21, No.5, May 1983, pp.645-664

[16] Tam, C.K.W., and Block, P.J.W., "On the Tones and Pressure Oscillations Induced by Flow Over Rectangular Cavities", Journal of Fluid Mechanics, Vol.89, Part 2, 1978, pp.373-399

[17] Rossiter, J.E., "Wind Tunnel Experiments on the Flow Over Rectangular Cavities at Subsonic and Transonic Speeds", ARC R&M No.3438, October 1964

[18] Komerath, N.M., Ahuja, K.K., and Chambers, F.W., "Prediction and Measurement of Flows Over Cavities- A Survey", AIAA Paper No. 87-0166, January 1987

[19] Chen, C.H., "Study of Subsonic and Transonic Flow Separation - With and Without Upstream Influence", Doctoral Dissertation, University of Tennessee, Knoxville, 1975

[20] Naudascher, E., "From Flow Stability to Flow Induced Excitation", Pro. ASCE, Journal of Hydraulics Div, Vol.93, No.HY4, Proceedings Paper 5336, July 1967, pp.15-40

[21] Rockwell, D., and Naudascher, E., "Review - Self Sustaining Oscillations of Flow Past Cavities", ASME Journal of Fluids Engineering, Vol.100, No.2, June 1978, pp.152-165

[22] Wilcox, F.J.Jr, "Passive Venting System for Modifying Cavity Flow Fields at Supersonic Speeds", AIAA Journal, Vol.26, No.3, March 1988, pp.374-376

[23] Sarohia, V., and Massier, P.F., "Control of Cavity Noise", AIAA Journal of Aircraft, Vol.14, No.9, September 1977, pp.833-837

[24] Franke, M.E., and Carr, D.L., "Effect of Geometry on Open Cavity Flow Induced Pressure Oscillations", AIAA Paper No. 75-492, March 1975

[25] Heller, H.H., and Bliss, D.B., "The Physical Mechanism of Flow Induced Pressure Fluctuations in Cavities and

Concepts for their Suppression", AIAA Paper No. 75-491, March 1975

[26] Smith, R.A., Gutmark, E., and Schadow, K.C., "Mitigation of Pressure Oscillations Induced by Supersonic Flow Over Slender Cavities", AIAA Paper No. 90-4019, October 1990

[27] Vakili, A.D., Wu,J.M., and Taylor, M., "Shear Flow Control Applied to Suppress Cavity Oscillations and Improve Store Separation", Weapons Carriage and Separation Workshop, Wright Patterson AFB, Dayton OH,April 1988

[28] Vakili, A.D., and Gauthier, C., "Control of Cavity Flow by Upstream Mass Injection", AIAA Journal of Aircraft, Vol.31, No.4, January-February 1994, pp.169-174

[29] Fernandez, F.L., and Zukoski, E.E., "Experiments in Supersonic Turbulent Flow with Large Distributed Surface Injection", AIAA Journal, Vol.7, No.9, September 1969, pp.1759-1767

[30] Blair, A.B.Jr, and Stallings, R.L., "Supersonic Axial Force Characteristics of a Rectangular-Box Cavity with Various Length-to-Depth Ratios in a Flat Plate", NASA TM-87659, April 1986

[31] Plumblee, H.E., Gibson, J.S., and Lassiter, L.W., "A Theoretical and Experimental Investigation of the Acoustic Response of Cavities in an Aerodynamic Flow", WADD-TR-16-75, March 1962

[32] Heller, H.H., Holmes, D.G., and Covert, E.E., "Flow Induced Pressure Oscillations in Shallow Cavities", Journal of Sound and Vibration, Vol.18, No.4, 1971, pp.545-553

[33] Bilanin, A.J., and Covert, E.E., "Estimation of Possible Excitation Frequencies for Shallow Rectangular Cavities", AIAA Journal, Vol.11, No.3, March 1973, pp.347-351

[34] Sarohia, V., "Experimental Investigation of Oscillations in Flows Over Shallow Cavities", AIAA Journal, Vol.15, No.7, July 1977, pp.984-991

[35] Sarno, R.L., and Franke, M.E., "Suppression of Flow Induced Pressure Oscillations in Cavities", Journal of Aircraft, Vol.31, No.1, January-February 1994, pp.90-96

[36] Goldstein, R.J., Shavit, G., and Chen, T.S., "Film-Cooling Effectiveness with Injection through a Porous

Section", ASME Journal of Heat Transfer, August 1965, pp.353-361

[37] Hankey, W.L., and Shang, J.S., "Analysis of Pressure Oscillations in an Open Cavity", AIAA Journal, Vol.18, No.8, August 1980, pp.892-898

[38] Baysal, O., and Stallings, R.L., "Computational and Experimental Investigation of Cavity Flowfields", AIAA Journal, Vol.26, No.1, January 1988, pp.6-7

[39] Rizetta, D.P., "Numerical Simulation of Supersonic Flow Over a Three-Dimensional Cavity", AIAA Journal, Vol.26, No.7, July 1988, pp.799-807

[40] Suhs, N.E., "Unsteady Flow Computations for a Three-Dimensional Cavity with and without an Acoustic Suppression Device", AIAA Paper No. 93-3402, August 1993

[41] Shih, S.H., Hamed, A., and Yeuan, J.J., "Unsteady Supersonic Cavity Flow Simulations using coupled k-ε and Navier-Stokes Equations", AIAA Journal, Vol.32, No.10, October 1994, pp.2015-2021

[42] Cooper, G.K., and Sirbaugh, J.R., "PARC Code: Theory and Usage", AEDC TR-89-15, December 1989

[43] Ho, C.M., and Huerre, P., "Perturbed Free Shear Layers", Annual Review of Fluid Mechanics, Vol.16, 1984, pp.365-424

[44] Lambert, E.P., "Measurements of the Shear Layer Over a Cavity with and without Upstream Mass Injection", Masters thesis, University of Tennesee-Knoxville, August 1994

[45] Heller, H., and Bliss, D., "Aerodynamically Induced Pressure Oscillations: Physical Mechanisms and Suppression Concepts", Wright-Patterson Air Force Base, Ohio, AFFDL-TR-74-133, February 1975

[46] Kaufman, L.G.II, Maciulaitis, A., and Clark, R.L., "Mach 0.6 to 3.0 Flows Over Rectangular Cavities", AFWAL-TR-82-3112, May 1883

VITA

Robert Calvin Wolfe was born on August 18, 1965 in Kansas City, Missouri. He attended Fort Osage High School and graduated in May 1983. In September 1983 he enrolled at the University of Missouri-Rolla and graduated in May 1987 with a bachelors degree in mechanical engineering. He began attending the University of Tennessee Space Institute in January 1993 and graduated with a masters degree in mechanical engineering in May 1995.